Check for updates

Received: 19 December 2022 | Accepted: 11 February 2023

DOI: 10.1111/gcb.16682

RESEARCH ARTICLE

Global Change Biology WILEY

Spatial heterogeneity of global forest aboveground carbon stocks and fluxes constrained by spaceborne lidar data and mechanistic modeling

Lei Ma[1] | George Hurtt[1] | Hao Tang[2] | Rachel Lamb[3] | Andrew Lister[4] | Louise Chini[5] | Ralph Dubayah[1] | John Armston[5] | Elliott Campbell[6] | Laura Duncanson[1] | Sean Healey[7] | Jarlath O'Neil-Dunne[8] | Lesley Ott[9] | Benjamin Poulter[10] | Quan Shen[1]

[1]Department of Geographical Sciences, University of Maryland at College Park, College Park, Maryland, USA

[2]Department of Geography, National University of Singapore, Singapore

[3]Geographical Sciences, Maryland Department of the Environment, University of Maryland at College Park, College Park, Maryland, USA

[4]United States Department of Agriculture Forest Service Northern Research Station, Newtown Square, Pennsylvania, USA

[5]Geographical Sciences, University of Maryland at College Park, College Park, Maryland, USA

[6]Maryland Department of Natural Resources, Annapolis, Maryland, USA

[7]USDA Forest Service Rocky Mountain Research Station, Fort Collins, Colorado, USA

[8]Rubenstein School of Environment and Natural Resources, University of Vermont, Burlington, Vermont, USA

[9]NASA Goddard Space Flight Center, Global Modeling and Assimilation Office, Greenbelt, Maryland, USA

[10]NASA Goddard Space Flight Center, Greenbelt, Maryland, USA

Correspondence
Lei Ma, Department of Geographical Sciences, University of Maryland at College Park, College Park, MD, USA.
Email: lma6@umd.edu

Funding information
GEDI ST, Grant/Award Number: 80HQTR21T0013; NASA Contract, Grant/Award Number: NNL15AA03C; NASA-CMS, Grant/Award Number: 80NSSC21K1059

Abstract

Forest carbon is a large and uncertain component of the global carbon cycle. An important source of complexity is the spatial heterogeneity of vegetation vertical structure and extent, which results from variations in climate, soils, and disturbances and influences both contemporary carbon stocks and fluxes. Recent advances in remote sensing and ecosystem modeling have the potential to significantly improve the characterization of vegetation structure and its resulting influence on carbon. Here, we used novel remote sensing observations of tree canopy height collected by two NASA spaceborne lidar missions, Global Ecosystem Dynamics Investigation and ICE, Cloud, and Land Elevation Satellite 2, together with a newly developed global Ecosystem Demography model (v3.0) to characterize the spatial heterogeneity of global forest structure and quantify the corresponding implications for forest carbon stocks and fluxes. Multiple-scale evaluations suggested favorable results relative to other estimates including field inventory, remote sensing-based products, and national statistics. However, this approach utilized several orders of magnitude more data (3.77 billion lidar samples) on vegetation structure than used previously and enabled a qualitative increase in the spatial resolution of model estimates achievable (0.25°

This is an open access article under the terms of the Creative Commons Attribution-NonCommercial License, which permits use, distribution and reproduction in any medium, provided the original work is properly cited and is not used for commercial purposes.
© 2023 The Authors. *Global Change Biology* published by John Wiley & Sons Ltd.

to 0.01°). At this resolution, process-based models are now able to capture detailed spatial patterns of forest structure previously unattainable, including patterns of natural and anthropogenic disturbance and recovery. Through the novel integration of new remote sensing data and ecosystem modeling, this study bridges the gap between existing empirically based remote sensing approaches and process-based modeling approaches. This study more generally demonstrates the promising value of spaceborne lidar observations for advancing carbon modeling at a global scale.

KEYWORDS
ecosystem demography, forest aboveground carbon stocks and fluxes, GEDI ICESat-2, lidar canopy height, process-based model, spatial heterogeneity

1 | INTRODUCTION

Forest carbon is one of the largest and most uncertain terms in the global carbon budget (Friedlingstein et al., 2022). Historical changes in climate, CO_2, and land-use activities affect forest equilibrium at a range of spatial and temporal scales and lead to long-lasting impacts on future carbon balance (Hurtt et al., 2002; Krause et al., 2020; McGuire et al., 2001; Thom et al., 2018). Characterizing those impacts and predicting future carbon dynamics is therefore a major challenge to the global carbon cycle research community. Addressing this challenge requires the development of advanced models able to ingest new forms of remote sensing data to better characterize the spatial heterogeneity in structure and function of forest ecosystems.

Over the past several decades, terrestrial ecosystem modeling has advanced to become a powerful tool for global analyses because it can be used to characterize essential ecological processes, including biophysics, plant physiology, population dynamics, plant biogeography, and biogeochemistry from local to global scales (Fisher et al., 2018; Prentice et al., 2007; Scheiter et al., 2013). With such broad capabilities, these process-based models can help quantify forest dynamics, understand complex interactions between terrestrial ecosystems and atmosphere, and attribute large-scale carbon dynamics to potential drivers (Ahlström et al., 2012; Quesada et al., 2018; Sitch et al., 2008, 2015). Many current models are core components of Earth system models and global carbon budgets, two important model frameworks used to study both short- and long-term terrestrial carbon dynamics (Eyring et al., 2016; Taylor et al., 2012).

However, model predictions are limited not only by model formulation and forcing data, but also by characterization of initial conditions. For global carbon cycle studies, the primary approach to estimating the current state of terrestrial ecosystems has been through the development and use of global land-use history reconstructions able to track the past land-use transitions and that give rise to secondary forests (Chini et al., 2021; Hurtt et al., 2002, 2006, 2011, 2020; Jones et al., 2016; Lawrence et al., 2016; Ma et al., 2020). The most recent version of the approach (i.e., LUH2) harmonizes multiple sources of information to resolve land-use transitions at 0.25° annual fractional coverage globally 850–2100 (Hurtt et al., 2020). These reconstructions, together with other forcing data (e.g., climate, atmospheric CO_2 concentration), are used in process-based ecosystem models to track historic forest changes and estimate current conditions, and then subsequently run forward to provide future projections (Eyring et al., 2016; Sitch et al., 2015; Taylor et al., 2012). While this approach has been proven useful for large-scale studies at relatively coarse spatial resolution, the challenge remains to initialize models using direct observations of forest structure.

Two advances offer a new way to address this challenge. First, lidar observations of 3D vegetation structure have been shown to provide direct and accurate measurement of forest vertical structure and serve as a proxy for measurement of aboveground carbon stocks (Drake et al., 2002; Dubayah et al., 2010; Dubayah & Drake, 2000; Huang et al., 2019; Los et al., 2012; Tang et al., 2012, 2021). Second, height-structured ecosystem models have advanced with an emphasis on explicit characterization of individual-based dynamics and forest vertical structure (Fisher et al., 2018; Hurtt et al., 1998; Longo et al., 2019; Ma et al., 2022; Medvigy et al., 2009; Moorcroft et al., 2001). Used together, these tools have provided powerful constraints on both aboveground carbon stocks and net carbon fluxes, and facilitated projections of forest carbon sequestration potential over heterogeneous landscapes (Antonarakis et al., 2011; Hurtt et al., 2004, 2019; Ma et al., 2021; Rödig et al., 2017). Originally studied at La Selva Biological Station in Costa Rica, high-resolution airborne lidar data were used in the Ecosystem Demography (ED) model to move beyond potential vegetation and map the aboveground biomass and net carbon fluxes of the forest (Hurtt et al., 2004). Subsequently, the approach was refined and applied to other sites, and extended to regional scales (Hurtt et al., 2010, 2016, 2019; Thomas et al., 2008). The most recent versions of the approach cover the 11-state Regional Greenhouse Gas Initiative region in northeastern United States (Ma et al., 2021), and have been approved for use in the U.S. state of Maryland's greenhouse gas inventory and climate action plan (MDE, 2021, 2022).

The recent emergence of spaceborne lidar missions, such as GEDI (Global Ecosystem Dynamics Investigation) and ICESat-2 (ICE, Cloud, and Land Elevation Satellite 2), provide unprecedented global observations of forest structure (Dubayah et al., 2020; Markus et al., 2017). In parallel, a global version of the ED model (ED v3) has recently been developed and evaluated for its performance with

13652486, 2023, 12, Downloaded from https://onlinelibrary.wiley.com/doi/10.1111/gcb.16682 by Readcube (Labtiva Inc.), Wiley Online Library on [01/07/2024]. See the Terms and Conditions (https://onlinelibrary.wiley.com/terms-and-conditions) on Wiley Online Library for rules of use; OA articles are governed by the applicable Creative Commons License

respect to modeling carbon dynamics, using comprehensive benchmarking datasets (Ma et al., 2022). The goal of this study was to combine these advances to quantify the spatial heterogeneity of forest structure and its impacts on global forest carbon stocks and fluxes.

2 | METHODS AND DATA

The methodological framework for this study includes three major components: model simulations using the ED model, generation of canopy height histogram from lidar data, and model initialization linking these products together (Figure 1). Resulting products are evaluated against reference datasets at a variety of scales. Below will describe each of these components.

2.1 | Ecosystem demography (ED) model

ED is an individual-based prognostic ecosystem model that integrates submodules of growth, mortality, hydrology, carbon cycle, and soil biogeochemistry (Hurtt et al., 1998; Moorcroft et al., 2001). ED can characterize plant dynamics at individual levels including growth, mortality, reproduction, and competition for light, water and nutrients. ED can also simulate the carbon cycle, including carbon uptake by leaf photosynthesis to carbon allocation for growth in leaves, roots, stem, and seedlings, as well as carbon decomposition in various soil carbon pools. The model can further characterize changes in individual plant density and composition under natural disturbance and land-use and land-cover change. Versions of the model have been used in multiple studies characterize regional carbon dynamics in response to climate change, elevated CO_2 concentration, land-use and land-cover change, and natural disturbance (Fisk et al., 2013; Flanagan et al., 2016; Hurtt et al., 2002; Longo et al., 2019; Medvigy et al., 2009).

A key feature distinguishing ED from most other process-based ecosystem models is its explicit track of vertical structure during ecosystem succession. Specifically, each plant has its own structural attributes such as associated canopy height and diameter at breast height. Canopy height dynamics are then tracked as a result of competition between plants and cumulative carbon balance between photosynthesis and respiration with given environmental conditions (e.g., temperature, precipitation, radiation, and soil moisture). Explicitly tracking canopy height under this framework can link the model simulation with external forest structure data from either remote sensing observations or field measurements.

This study used a global version of ED (v3.0) which has been developed and calibrated at global scale (Ma et al., 2022). This version has also been benchmarked by a series of datasets including spatial distribution of plant function types, carbon stocks in vegetation and soil, carbon and water fluxes, and vegetation structures across a range of spatial and temporal scales. More details about model development and evaluation (v3.0) can be found in Ma et al. (2022).

2.2 | Lidar data

GEDI, launched in December 2018 from the International Space Station (ISS), is a high-resolution laser specifically designed for forest

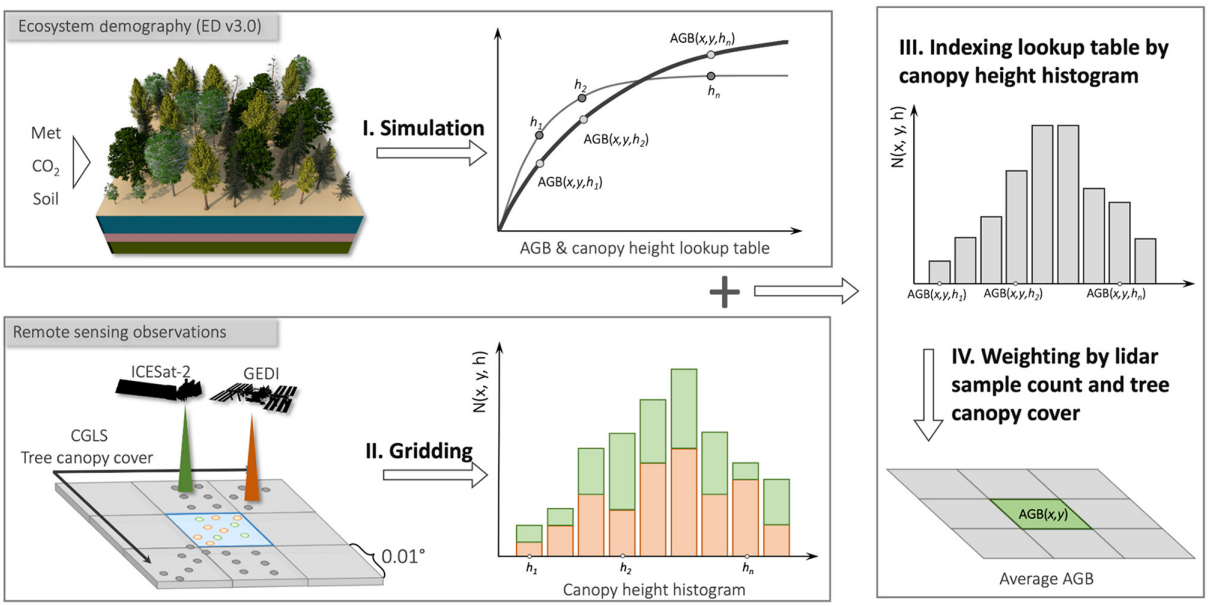

FIGURE 1 Illustration of ED-Lidar initialization using inputs of canopy height histogram and tree canopy cover grid. The top box depicts the generation of AGB-height lookup tables by running ED with drivers of meteorology, CO_2, and soil properties. The bottom box depicts generation of gridded canopy height histograms from GEDI and ICESat-2 observations and average tree cover from the CGLS product for the blue grid. Color circles represent GEDI and ICESat-2 footprint/segment-level observations. The right box depicts the generation of average AGB for a grid cell using the height-based initialization approach.

13652486, 2023, 12, Downloaded from https://onlinelibrary.wiley.com/doi/10.1111/gcb.16682 by Readcube (Labtiva Inc.), Wiley Online Library on [01/07/2024]. See the Terms and Conditions (https://onlinelibrary.wiley.com/terms-and-conditions) on Wiley Online Library for rules of use; OA articles are governed by the applicable Creative Commons License

vertical structure measurements (Dubayah et al., 2020). ICESat-2, launched in September 2018, is a free-fly satellite aiming to measure surface elevation over the entire globe and vegetation height over land (Markus et al., 2017; Neuenschwander & Pitts, 2019). Both NASA missions are collecting samples over their own designed tracks and spatial domains. Because it is mounted on the ISS, GEDI only covers latitudes of 51°N–51°S, but with more frequent orbits and sampled surface areas than ICESat-2. Neither mission provides wall-to-wall coverage at the native resolution of their measurements (25 m footprint for GEDI and 100 m segment for ICESat-2).

In order to align data from the two lidar missions, which have different spatial characteristics, the footprint/segment canopy height observations provided by the GEDI L2A (Dubayah et al., 2021) and ICESat-2 ATL08 (Neuenschwander et al., 2021) products were summarized within 0.01° grid cells to maximize the spatial coverage and sample density. Gridded canopy height histograms, average canopy height, and sample density were produced for each lidar source separately and for their combination. Information contained in the gridded canopy height histogram was used as input data for the ED initialization, the average canopy height was used to assess the consistency of two missions, and lidar sampling density was used to assess the current data spatial coverage. To quantitatively assess the spatial coverage over forest (tree canopy cover above 1%), the total land areas of 0.01° grid cells that have lidar samples were calculated by latitude.

The gridding process of the canopy height histogram included quality filtering of lidar samples, locating to 0.01° cell using recorded coordinates, and binning the resulting samples, per cell, into a histogram with bin values ranging from 5 m to 50 m with an equal bin size of 0.5 m. The resulting canopy height histograms were thus, in effect, converted to maps with 90 layers (90 bins per histogram per cell), and each layer records the lidar sample count within the range of the height bin. In addition, map layers associated with average canopy height and sample point density within each cell were generated. Canopy height metrics used for gridding were the RH100 attribute from GEDI L2A product, and h_canopy attribute from ICESat-2 ATL08 product. For both GEDI and ICESat-2, only footprints/segments that meet each filtering criteria were used for gridding. For GEDI, the filtering criteria were: (1) quality_flag = 1; (2) sensitivity >0.95; and (3) RH100 > 5 m. For ICESat-2, the filtering criteria were: (1) dem_removal_flag = 0; (2) canopy_flag = 1; (3) cloud_flag_atm <4; and (4) h_canopy >5 m. The filtering criteria were established to exclude bad observations or those over non-forest areas. The height threshold great than 5 m was also used in the FAO definition of forests. Table 1 summarizes details of product versions, acquisition time, and number of granules used for gridding.

2.3 | Model initialization

To link lidar observations to the ED model, the model initialization followed a height-based look-up table approach modified here for use of spaceborne lidar data (Figure 1). The initialization approach was first proposed in Hurtt et al. (2004) and subsequently applied in regional applications using aircraft lidar data with wall to wall coverage (Hurtt et al., 2010, 2016, 2019; Ma et al., 2021; Thomas et al., 2008). In essence, the approach used tree canopy height in the model as an indicator of forest successional state under the assumption that trees grow taller in size as they develop (Botkin et al., 1972; Saldarriaga et al., 1988; Shugart, 1984; Shugart &

TABLE 1 Summary of datasets used for ED simulation, initialization, and evaluation of AGB estimates.

Variable	Source	Description	References
ED drivers			
Meteorology	MERRA2	Global gridded, 0.5°, 2011–2020	Gelaro et al. (2017)
CO_2	NOAA CarbonTracker	400 ppm, spatial and temporal constant	Jacobson et al. (2020)
Soil properties	Montzka et al. (2017)	Global gridded, 0.5°	Montzka et al. (2017)
ED-Lidar initialization input			
Canopy height	GEDI L2A (v002)	51° N–51° S, 20 m footprint, 43,716 granules during 2019 March–2021 August	Dubayah et al. (2021)
	ICESat-2 ATL08 (v05)	Global, 100 × 20 m segment, 165,990 granules during 2018 October–2021 October	Neuenschwander et al. (2021)
Tree canopy cover	CGLS	Global gridded, 100 m, 2019	Buchhorn et al. (2020)
AGB stocks and fluxes evaluation			
AGB stocks	GEDI L4B	51° N–51° S, 20 footprint, 44,095 granules during 2019 April–2021 August	Dubayah et al. (2022)
	GlobBiomass	Global, 100 m, 2010	Santoro (2018)
	ESA CCI	Global, 100 m, 2018	Santoro and Cartus (2021)
	FAO FRA	Global, country, 2020	FAO (2020)
	USFS FIA	US CONUS, hexagon (~640 km^2), 2010–2019	Menlove and Healey (2020)
AGB stocks and fluxes	ED-LUH2	Global, 0.5°, 2019 and 10 years forward	Ma et al. (2022)

13652486, 2023, 12, Downloaded from https://onlinelibrary.wiley.com/doi/10.1111/gcb.16682 by Readcube (Labtiva Inc.), Wiley Online Library on [01/07/2024]. See the Terms and Conditions (https://onlinelibrary.wiley.com/terms-and-conditions) on Wiley Online Library for rules of use; OA articles are governed by the applicable Creative Commons License

West, 1977). Here, considering the sample-based nature of GEDI and ICESat-2 data, a new initialization approach, using the canopy height histogram, captured sub-grid cell variability of heights.

Following previous studies, a look-up table produced by ED (v3.0) was used to connect lidar observations of canopy height to model simulations of potential canopy height and structure. The look-up table consisted of a time series of modeled potential vegetation structure (i.e., canopy height, AGB, GPP, etc.) for each grid cell from bare ground to old-growth indexed by canopy height. Inputs included meteorological forcings, soil characteristics, and atmospheric CO_2 concentration (Table 1). Meteorological forcing data came from the NASA Modern-Era Retrospective analysis for Research and Applications, Version 2 (MERRA-2; Gelaro et al., 2017). Variables of surface air temperature, surface specific humidity, incident shortwave radiation, wind speed, precipitation, and multi-layer soil temperature were spatially interpolated to 0.5° and averaged to monthly diurnal estimates. Soil hydraulic properties came from Montzka et al. (2017), which provides spatial parameter maps of soil depth and saturated hydraulic conductivity. CO_2 was held spatially and temporally constant at 400 ppm (Jacobson et al., 2020). Furthermore, the disturbance rate was set as 1.2% for the whole global domain except ecoregions on the western North America, which are home to tallest and long-lived species (e.g., redwood, coast Douglas-fir). For these areas, 0.5% of the disturbance rate was used. All plant functional types were set with an equal seedling density over the globe.

More specifically, the initialization used the look-up table to estimate AGB stocks for the tree fraction of each 0.01° grid cell (Figure 1). The first step was to use the lidar data to index the lookup table and find the corresponding model AGB (Ma et al., 2021). The indexing step was implemented for each bin of the observed canopy height histogram within each grid. Next, the AGB of each bin was weighted by the associated lidar sample count in that grid cell to produce the average AGB. Finally, the average AGB for the whole grid cell was computed by weighting by tree cover fraction. Tree canopy cover was derived from Copernicus Global Land Service (CGLS; Buchhorn et al., 2020). The forest fraction in 2019 from CGLS was aggregated to 0.01° by averaging all 100 m CGLS grid cells in each 0.01° grid cell. For AGB fluxes, ED was then run forward for 10 years. This forward simulation took into account potential natural disturbance and fire but not changes in climate, CO_2, or land use. The resulting flux therefore represents potential net aboveground carbon fluxes under these controlled conditions, accounting for forest successional state but without losses from land-use change and impacts of climate and CO_2 fertilization.

The initialization can be expressed as follows:

$$\mathrm{AGB}\,(x,y) = \frac{\sum_{h=5}^{50} \mathrm{AGB}(x,y,h) \times N(x,y,h)}{\sum_{h=5}^{50} N(x,y,h)} \times C(x,y) \qquad (1)$$

where $\mathrm{AGB}\,(x,y)$ is average AGB stocks at a 0.01° grid cell at location of x and y, $\mathrm{AGB}(x,y,h)$ is AGB from indexing lookup table with lidar canopy height h, $N(x,y,h)$ is lidar sample count at the grid cell of height bin h, and $C(x,y)$ is the tree canopy cover of the grid cell. Hereafter for simplicity, the estimates of AGB stocks and potential net AGB fluxes from this initialization were referred to as ED-Lidar carbon stocks and carbon fluxes. In the default case, the ED-Lidar used GEDI and ICESat-2 combined unless the lidar source was explicitly pointed out.

2.4 | Model evaluation

ED-Lidar estimates of carbon stocks and fluxes were evaluated by multiple reference datasets at various spatial scales and domains. These datasets were derived from different methods including a sample-based forest inventory, remote sensing empirical approaches, and ecosystem modeling as summarized in Table 1.

For carbon stocks, the reference data included four major sources: (1) gridded remote sensing-based AGB maps, (2) inventory data from US Forest Service Forest Inventory Analysis (FIA), (3) national statistics from Global Forest Resources Assessment (FRA) in 2020 by the Food and Agriculture Organization (FAO), and (4) estimates from ED initialization with LUH2. These datasets vary in spatial resolution and domain (Table 1). The first source included three gridded remote sensing-based maps, namely GEDI L4B (Dubayah et al., 2022), the ESA CCI (Santoro & Cartus, 2021), and the GlobBiomass (Santoro, 2018). Specifically, the GEDI product provided a gridded map at a spatial resolution of 1 km over latitudes between 51°N and 51°S. The product relied on original GEDI observations of canopy height without spatial extrapolation with auxiliary data using machine learning algorithms. The ESA CCI and GlobBiomass products provided wall-to-wall estimates at a spatial resolution of 100 m. These two products employed machine learning to extrapolate AGB estimates from locations with sparse lidar measurements or ground measurements to wall-to-wall coverage using optical and radar remote sensing data. The ESA CCI and GlobBiomass were aggregated to 0.01° by averaging all 100 m grid cells. The second source was the USFS FIA data which were used here from the database developed by Menlove and Healey (2020). This database aggregated forest inventory data from nearly 327,000 field plots to over 12,000 hexagons over the conterminous United States. Aggregation of FIA plot data to larger, hexagonal areas lessens concerns about spatial mismatch between plots and pixels and landowner privacy. Only hexagons with forest proportion larger than 1% and more than 12 plots were used. The third data source, the 2020 FAO FRA (FAO, 2020), includes multiple country-reported forest statistics. These estimates vary in the quality and accuracy depending on the country's inventory capabilities. In this study, the country's total forest aboveground carbon stocks were computed by multiplying the country's reported total forest area by the reported average forest AGB. In total, 178 countries were included by excluding countries that neither report the forest area nor the average AGB. The fourth source is from ED initialization with LUH2, the details will be described below.

13652486, 2023, 12, Downloaded from https://onlinelibrary.wiley.com/doi/10.1111/gcb.16682 by Readcube (Labtiva Inc.), Wiley Online Library on [01/07/2024]. See the Terms and Conditions (https://onlinelibrary.wiley.com/terms-and-conditions) on Wiley Online Library for rules of use; OA articles are governed by the applicable Creative Commons License

For carbon fluxes, corresponding reference data were more limited due to compatibility. The most comparable reference data were from carbon cycle models driven by land-use history. To isolate the impact of the initialization approach itself, ED-LUH2 was used as a reference (Ma et al., 2022). ED-LUH2 used the same ED model version but was initialized with the LUH2 land-use history dataset following the approach commonly used in global carbon modeling that spins up processes-based ecosystem models with land-use history data. This initialization shared a similar experiment protocol to TRENDY and CMIP6 that employed thousands of years of simulation to initialize ecosystems from the pre-industrial era to present by taking into account climate change, rising CO_2 concentrations, and land-use change (Ma et al., 2022). In particular, the initialization consisted of two ED model runs at 0.5° (called equilibrium simulation and transient simulation). The first run drove ED for 1000 years from the bare ground conditions to equilibrium by which time vegetation composition and carbon pools of vegetation and soil had reached dynamic equilibrium. The second run restarted from the end of the equilibrium simulation and simulated for 1169 years, corresponding to the period AD 851–AD 2019, with varying CO_2 levels, land-use transitions, and climate variability. In our study, we used an updated version of LUH2 that was developed for the Global Carbon Budget report, which was similar to its predecessor. It included information on changes in agriculture and forest extent, shifting cultivation and wood harvesting, among others (Chini et al., 2021). Once initialized, ED was run forward for 10 years by taking into account only natural disturbance and fire but not changes in climate, CO_2 concentration, and land use, similar to the abovementioned forward simulation of ED-Lidar (Section 2.3). The resulting AGB stocks in 2019 and average AGB fluxes of 10 years forward simulation was used in the following comparison (hereinafter referred to as ED-LUH2).

3 | RESULTS

3.1 | Global patterns of forest canopy height

Global canopy height maps at a resolution of 0.01° were generated by gridding lidar shots from GEDI and ICESat-2 individually (Figure 2a,b). GEDI collected 2.14 billion of shots, covering about 76.96 million km^2 of 0.01° grid cells between latitudes 51°N and 51°S. Due to clustered ground tracks and dense sampling, GEDI covered the majority of forested grid cells in this domain (Figure 2a; Figure S1a). Coverage varied within the domain, with regions at relatively high latitude having nearly wall-to-wall spatial coverage (Figure 2a) and high lidar sample density (Figure 2c) at this resolution. On average, GEDI had a sample density of 19.58 shots per grid cell (Figure S1b). In comparison, ICESat-2 collected 1.63 billion of shots, covering 77.84 million km^2 over the whole globe. ICESat-2 coverage varied more strongly with latitude (Figure 2b; Figure S1b) and had lower lidar sample density than GEDI (Figure 2d). On average, ICESat-2 had a sample density of 10.56 shots per grid cell.

Gridded average canopy height from GEDI and ICESat-2 had a similar spatial distribution over the overlapping domain (Figure 2a,b) despite differences in coverage and sampling density (Figure 2c,d). Both maps show relatively tall canopy height in similar areas of tropical and temperate forest including: Amazon, Congo, Pacific Northwest, eastern North America, eastern Europe, eastern Himalayas, southern Asia, and the far east of Russia. They also similarly represented the spatial gradient from forest to savanna in South America and Africa. Meanwhile, both products produced height variation at sub-grid level (Figure S2). Note that the difference in the histogram and average height between two missions is expected as lidar samples might be taken from different proportions of a grid (i.e., sampling error) and also due to different lidar techniques.

Despite broad qualitative agreement, the two lidar sources have important technical differences in instruments (waveform based vs. photon based) and mapping units (footprint vs. segment) which necessitates quantitative comparison prior to use in initialization. The height agreement between GEDI and ICESat-2 was assessed by comparing the gridded average canopy height over grid cells sampled by both sources (>20 shots per grid cell; Figure S3). The comparison of ~12 million pairs revealed strong correlation between the two products (i.e., R^2 of .66, mean bias of 1.2 m, and RMSE of 3.96 m).

3.2 | Forest carbon stocks and fluxes

The gridded canopy height by combining GEDI and ICESat-2, and the carbon products from initialization are shown in Figure 3. The global and regional totals are presented first, followed by the spatial patterns of the results.

3.2.1 | Global and regional totals

The global aboveground carbon stocks were estimated as 250.24 Pg C. The stocks were 205.74 Pg C over latitudes 51°N–51°S, and 157.37 Pg C over latitudes 23°N–23°S. The stocks were 13.03 Pg C over US CONUS (Table 2). For carbon fluxes, the global total was 2.57 Pg C/year, and 2.42 Pg C/year over latitudes 51°N–51°S, 1.91 Pg C/year over latitudes 23°N–23°S, and 0.12 Pg C/year over US CONUS (Table 3).

The estimate of carbon stocks was compared to reference datasets including: GEDI L4B, ESA CCI, GlobBiomass, ED-LUH2, and USFS FIA over different spatial domains (Table 2). Generally, total carbon stocks from ED-Lidar were closer to GEDI L4B and ED-LUH2 than to ESA CCI and GlobBiomass. Over latitudes of 51°N–51°S, where data from all sources were available, the difference between ED-Lidar and GEDI L4B and ED-LUH2 was 33.09 Pg C and 27.51 Pg C, respectively. The corresponding differences from ESA CCI and GlobBiomass were larger, 46.99 Pg C and 37.31 Pg C, respectively. Zonally, ED-Lidar produced a similar relative zonal distribution to all three reference datasets available globally, ~62% between latitudes 23°N–23°S and ~82% between latitudes 51°N–51°S. Over US CONUS, ED-Lidar compared more favorably to ED-LUH2 and USFS FIA with differences smaller than 0.5 Pg C (~3%).

13652486, 2023, 12, Downloaded from https://onlinelibrary.wiley.com/doi/10.1111/gcb.16682 by Readcube (Labtiva Inc.), Wiley Online Library on [01/07/2024]. See the Terms and Conditions (https://onlinelibrary.wiley.com/terms-and-conditions) on Wiley Online Library for rules of use; OA articles are governed by the applicable Creative Commons License

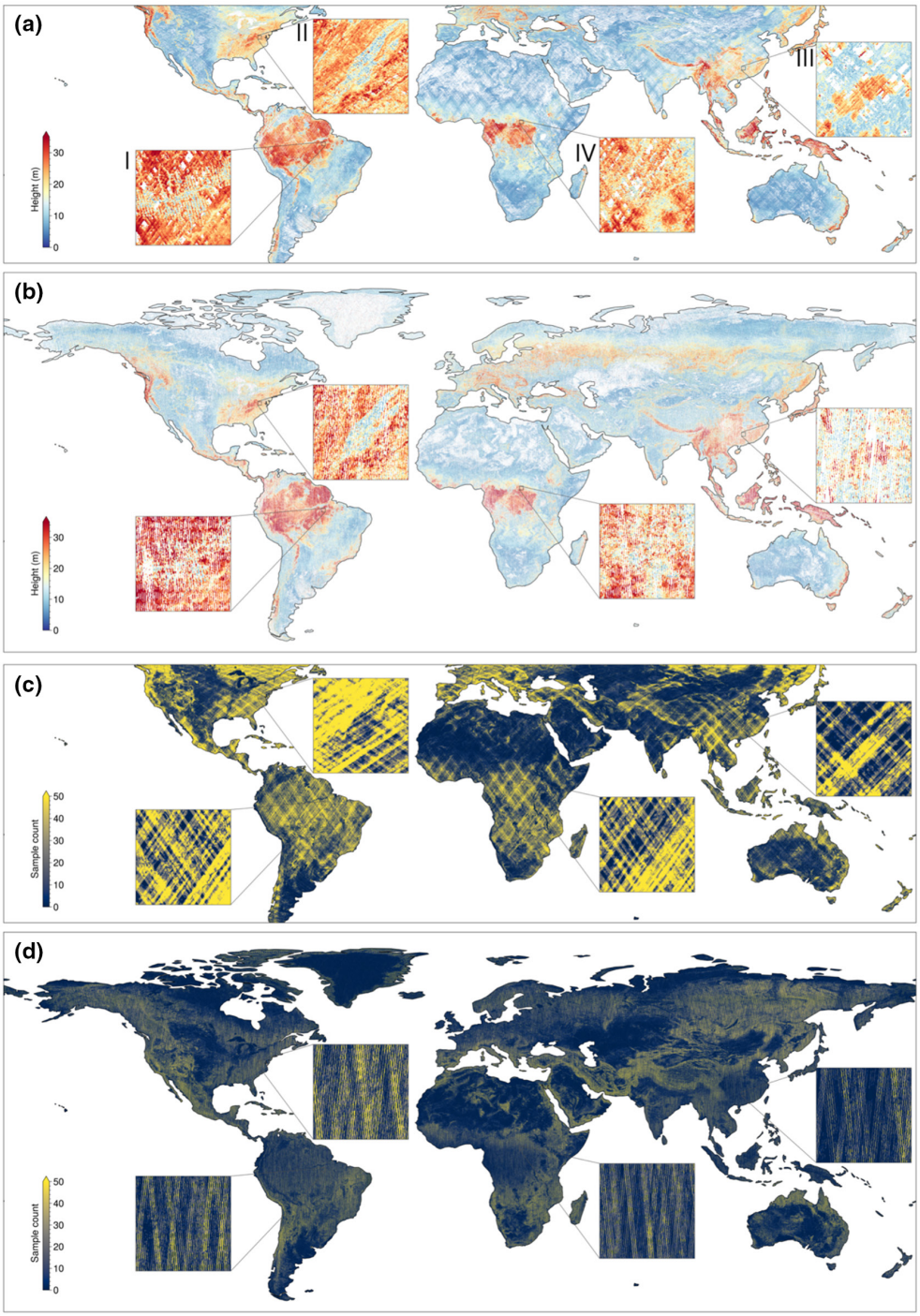

FIGURE 2 Average canopy height at 0.01° by gridding 3.77 billion footprint/segment-level observations from GEDI (a) and ICESat-2 (b) and associated sample density in (c) and (d). The insets in (a) and (b) highlight fine-scale spatial distribution and coverage gaps at selected regions.

Total carbon fluxes were compared between ED-Lidar and ED-LUH2. Globally, the total carbon fluxes from ED-Lidar were 2.57 Pg C/year. This was compared to corresponding estimates from ED-LUH2 initialization at 2.52 Pg C/year (Table 3). Despite the close global agreement, larger differences were present zonally. For example, ED-Lidar and ED-LUH2 estimated 74% and 54% of global fluxes in latitudes from 23°N to 23°S, respectively.

3.2.2 | Spatial distribution of carbon stocks and fluxes

Estimates of carbon stocks and fluxes revealed spatial patterns around the world. Regionally, relatively large carbon stocks estimates appeared in the tropical and temperate forest which have high canopy height (Figure 3a). In South America and central Africa,

13652486, 2023, 12, Downloaded from https://onlinelibrary.wiley.com/doi/10.1111/gcb.16682 by Readcube (Labtiva Inc.), Wiley Online Library on [01/07/2024]. See the Terms and Conditions (https://onlinelibrary.wiley.com/terms-and-conditions) on Wiley Online Library for rules of use; OA articles are governed by the applicable Creative Commons License

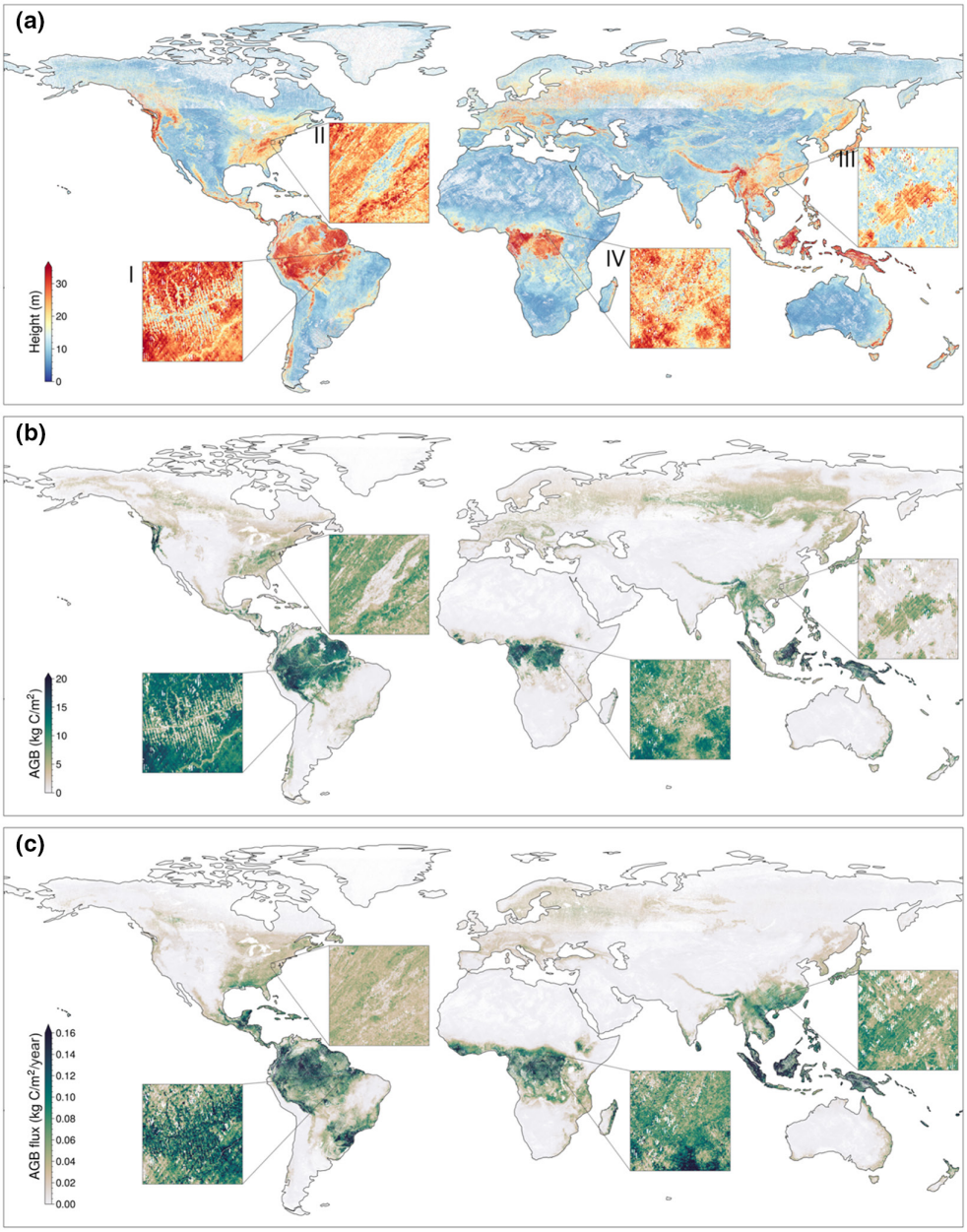

FIGURE 3 Average lidar canopy height at 0.01° in (a) by gridding both GEDI and ICESat-2 together, and carbon stocks (b) and fluxes in (c) from ED-Lidar (GEDI and ICESat-2 combined). The insets highlight fine-scale spatial distribution and coverage gaps at selected regions (1.5°×1.5°). Note that the three maps show grid-cell averages aggregated from sub-grid scale heterogeneity for each variable.

carbon stocks had a sharp gradient in the transition from forest to savanna. Analogous patterns were found for carbon fluxes, but were more complex (Figure 3b). Within biomes, there was generally an inverse relationship between carbon stocks and fluxes, whereas between biomes, carbon stocks and fluxes were positively correlated.

Estimates of carbon stocks and fluxes were characterized at fine scale, revealing enhanced sub-grid spatial heterogeneity around the world that was not tractable at coarse resolutions of prior modeling studies. Globally, these estimates have captured >25 times higher resolution (>600 times more grid cells) than modeling studies at 0.25° and >50 times higher resolution (>2500 more grid cells) than those at 0.5°. The increase in spatial resolution allowed relating spatial heterogeneity of carbon stocks and fluxes to potential causes. Here, four example areas were used as illustrations (insets in Figures 2 and 3). The first was the "fishbone" pattern in the Amazonian rainforests, a unique spatial pattern of deforestation. This was a result of forest clearing occurring in association with a network of highways and local roads and had resulted in fragmented landscape with a mixture of cropland, pasture, settlements, and left-over forest (Arima et al., 2016). The second and third examples were fragmented landscapes in eastern United States and southern China. In these areas, forest clearing for cropland and urban expansions had resulted in isolated and small forest fragments over the landscape (Liu et al., 2019;

13652486, 2023, 12, Downloaded from https://onlinelibrary.wiley.com/doi/10.1111/gcb.16682 by Readcube (Labtiva Inc.), Wiley Online Library on [01/07/2024]. See the Terms and Conditions (https://onlinelibrary.wiley.com/terms-and-conditions) on Wiley Online Library for rules of use; OA articles are governed by the applicable Creative Commons License

TABLE 2 Total carbon stocks by regions from ED initialization and other reference datasets.

Source	Total carbon stocks (Pg C)			
	Global	51°N–51°S	23°N–23°S	US CONUS
ED-Lidar initialization				
ED-GEDI-ICESat-2	250.24	205.74	157.37	13.03
ED-GEDI	n/a	196.53	149.11	13.11
ED-ICESat-2	268.96	224.47	173.30	12.95
Other estimates				
GEDI L4B	n/a	238.83	152.36	19.73
ESA CCI	315.23	252.73	195.77	16.10
GlobBiomass	293.06	243.05	182.08	16.39
ED-LUH2	272.80	233.25	166.40	13.37
USFS FIA	n/a	n/a	n/a	13.34, 16.39

TABLE 3 Total carbon fluxes by regions from ED-Lidar and ED-LUH2 initialization.

Source	Total carbon fluxes (Pg C/y)			
	Global	51°N–51°S	23°N–23°S	US CONUS
ED-Lidar initialization				
ED-GEDI-ICESat-2	2.57	2.42	1.91	0.12
ED-GEDI	n/a	2.60	2.07	0.12
ED-ICESat-2	2.27	2.12	1.64	0.12
Other estimates				
ED-LUH2	2.52	2.23	1.37	0.19

Riitters et al., 2002). The fourth example was a mixed forest–savanna landscape in Africa. This was the most widespread ecotone in tropical areas that shows sharp boundaries in tree cover as results of multiple factors (e.g., rainfall, fire, species; Oliveras & Malhi, 2016). The estimates of carbon stocks and flux produced here at 0.01° at global scale likely revealed the same kind of spatial details elsewhere.

For validation, the spatial patterns of ED-Lidar carbon stocks and fluxes were first compared to those of other sources by latitude. Estimates of carbon stocks from ED-Lidar produced a latitudinal gradient similar to other datasets, peaking at the equator and decreasing toward higher latitudes (Figure 4a). However, the difference between ED-Lidar and other datasets varied with latitudes and by comparison data source. Estimates of carbon flux from ED-Lidar also shared similar gradients in comparison to that of ED-LUH2, with flux in the tropics being two times larger than over higher latitudes (Figure 4b). The major difference is that ED-Lidar was higher than ED-LUH2 in the tropics but lower over latitudes above 20°N. Over the Amazon and Congo rainforests, estimates of carbon stocks from ED-Lidar at the grid-cell scale, were relatively lower than those from ESA CCI (Figure 5c,d) and ED-LUH2 (Figure 5g,h) and relatively higher than those from GEDI L4B (Figure 5a,b) and GlobBiomass (Figure 5e,f). Over African savannas, ED-Lidar estimates were lower than all other comparison datasets except ED-LUH2. Over Northeast Siberian forests, ED-Lidar estimates were higher than ESA CCI, GlobBiomass, and ED-LUH2. Estimates of carbon flux from ED-Lidar showed relatively higher fluxes over central Amazon rainforests and African savannas and lower fluxes over Europe (Figure 5i,j).

Next, spatial patterns of ED-Lidar carbon stocks and fluxes were compared to other estimates at various spatial scales where reference data were available (0.01° grid cell, hexagon, and country). Overall, estimates of carbon stocks from ED-Lidar correlated with other estimates with R^2 ranging from .68 to .73, RMSE ranging from 1.97 to 2.24 kg C/m^2, and bias ranging from −0.57 to −0.21 kg C/m^2 (Figure 6a–d). Comparison to GEDI L4B indicated that there was strong correlation over all carbon stock values despite relatively higher values in ED-Lidar (Figure 6a). Such correlation became weaker in comparison to ESA CCI, GlobBiomass, and ED-LUH2 (Figure 6b–d). For example, ED-Lidar exhibited larger variations than GlobBiomass and ED-LUH2 for carbon stocks exceeding 10 kg C/m^2 (Figure 6c,d). The estimates of carbon flux from ED-Lidar showed relatively low correlation with ED-LUH2 (Figure 6e).

At the hexagon scale over the US CONUS domain (Figure 7), carbon stocks varied regionally similar to USFS FIA data with higher carbon stocks estimates from ED-Lidar in the Pacific northwest and Appalachian Mountains (Figure 7a,b). Scatter plot comparisons suggested high correlation between ED-Lidar estimates and FIA data, with R^2 of approximately 0.7, bias of about −0.5 kg C/m^2, and RMSE of about 1.5 kg C/m^2 (Figure 7d). Regionally, ED-Lidar had lower values in northeastern and midwest regions, and higher values in the northwestern region.

At the country scale, ED-Lidar was compared to total forest carbon stocks from FAO FRA 2020 (Figure 8). ED-Lidar and the FRA estimate were highly correlated (R^2 of .94, bias of −0.03 Pg C, and RMSE of 1.05 Pg C). In addition, ED-Lidar and FRA estimates were very similar for countries with the largest stocks such as Brazil, Russia, the United States, and Democratic Republic of the Congo, with relative differences between 3% and 12%. ED-Lidar was slightly higher than FRA for Indonesia and China and lower for Canada.

13652486, 2023, 12, Downloaded from https://onlinelibrary.wiley.com/doi/10.1111/gcb.16682 by Readcube (Labtiva Inc.), Wiley Online Library on [01/07/2024]. See the Terms and Conditions (https://onlinelibrary.wiley.com/terms-and-conditions) on Wiley Online Library for rules of use; OA articles are governed by the applicable Creative Commons License

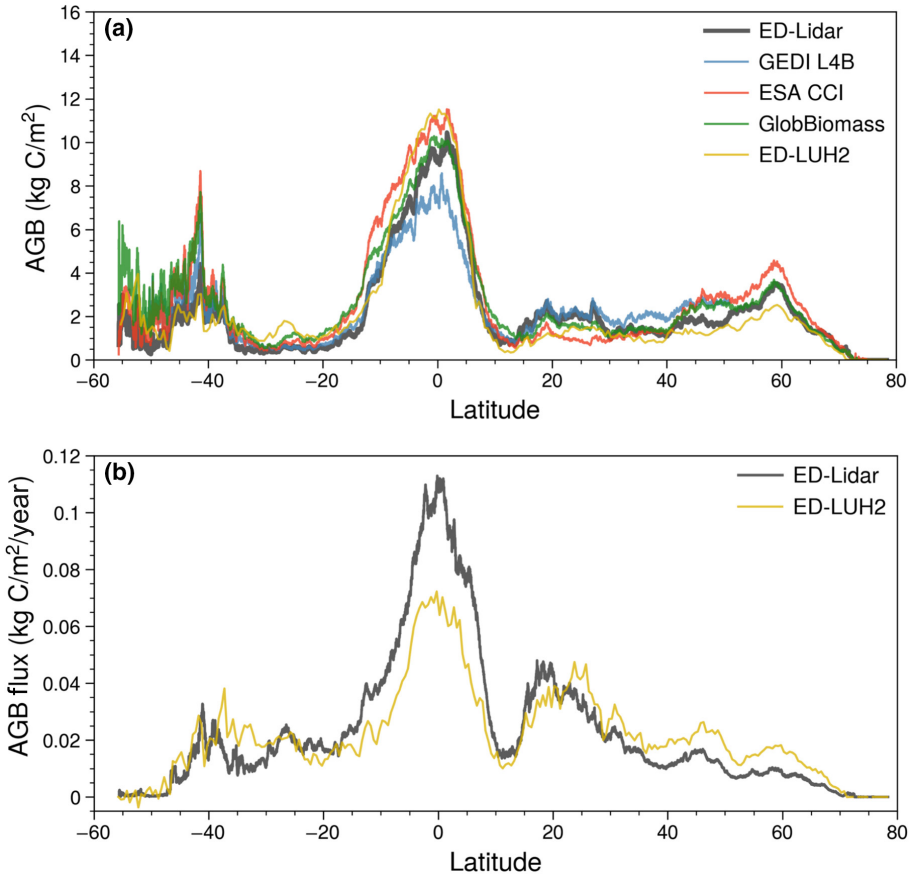

FIGURE 4 Comparison of latitudinal average of average carbon stocks (a) and fluxes (b) between ED-Lidar and other reference datasets. Estimates from ED-Lidar and other datasets are made within 0.01° grid cells and averaged by latitude zone except ED-LUH2.

Finally, to assess the impact of lidar data source, the results from model initialization were compared using GEDI alone and ICESat-2 alone (Figures S4 and S5). Generally, ICESat-2 sampled a larger spatial domain enabling broader coverage for model initialization, whereas GEDI provided higher shot density enabling more detailed coverage. The global domain sampled by ICESat-2 represented 72.43 Pg C more carbon than the GEDI domain alone (Table 2). However, over the GEDI domain, the results indicated that initialization was slightly better than with ICESat-2 alone relative to USFS FIA data (Figure S6). Analogous comparisons to GEDI L4B suggested a similar result (Figure S7).

4 | DISCUSSION AND CONCLUSIONS

Decades of carbon cycle studies have advanced knowledge of terrestrial carbon stocks and fluxes. However, these terms remain among the most uncertain in global carbon budgets, and are even more uncertain when estimated at the higher spatial resolutions needed for carbon monitoring and process-level understanding (Anav et al., 2013; Houghton, 2003, 2020; Liu et al., 2011; Yang et al., 2020). Standard global terrestrial ecosystem modeling studies have relied on long-term model simulations driven by land-use history reconstruction to track the anthropogenic land-use and land-cover changes needed to track historical fluxes and estimate contemporary conditions (Eyring et al., 2016; Hurtt et al., 2006, 2011, 2020; Lawrence et al., 2016; Ma et al., 2020; Sitch et al., 2008, 2015; Taylor et al., 2012). The most recent version of data driving this approach involved 12 land-use classes, resolved at 0.25 degree resolution, and reconstructed over 1100 years (Chini et al., 2021; Hurtt et al., 2020). In parallel, other studies have noted the promise of new satellite missions deploying lidar to advance carbon stock and flux mapping, particularly at higher spatial resolutions (Baccini et al., 2012; Dubayah et al., 2022; Harris et al., 2021; Saatchi et al., 2011; Santoro, 2018; Wang et al., 2021; Xu et al., 2021).

In this study, we developed a new approach to integrate canopy height data derived from spaceborne lidar observations and tree cover fraction data derived from optical remote sensing into a height-based ecosystem model to constrain representation of contemporary forest conditions and associated carbon stocks and fluxes, and compare to the land-use history driven approach. Results across a range of reference datasets suggested that lidar-based initialization produced carbon stocks and fluxes estimates comparable to reference datasets across a range of spatial scales/domains. However, with this new approach, literally billions of measurements of vegetation structure were used to constrain and map contemporary forest carbon stocks and fluxes at an unprecedented spatial resolution of 0.01° globally.

13652486, 2023, 12, Downloaded from https://onlinelibrary.wiley.com/doi/10.1111/gcb.16682 by Readcube (Labtiva Inc.), Wiley Online Library on [01/07/2024]. See the Terms and Conditions (https://onlinelibrary.wiley.com/terms-and-conditions) on Wiley Online Library for rules of use; OA articles are governed by the applicable Creative Commons License

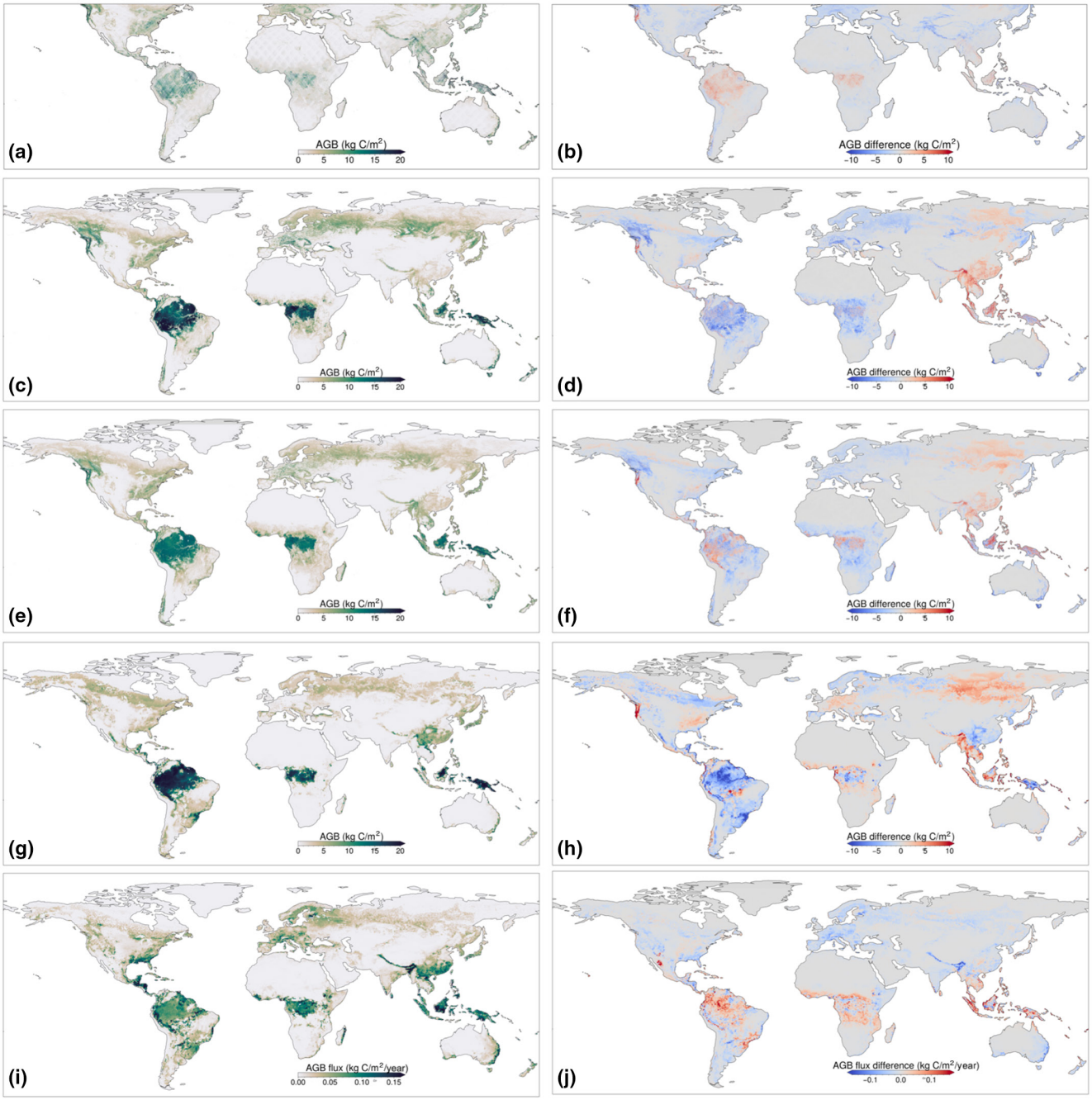

FIGURE 5 Comparison of carbon stocks and fluxes between ED-Lidar and other reference datasets. (a), (c), (e), and (g) are carbon stock estimates from GEDI L4B, ESA CCI, GlobBiomass, and ED-LUH2, respectively, (i) are carbon fluxes estimates from ED-LUH2. (b), (d), (f), (h), and (j) are spatial differences between ED-Lidar with each of the four datasets (ED-reference). Note that in comparison to ED-LUH2 (h and j), ED-Lidar estimates were aggregated to 0.5°.

The benefits of the improved approach and high spatial resolution are many. Foremost, increased spatial resolution reduces potential model averaging errors (Hurtt et al., 2010). Spatial heterogeneity in vegetation structure interacts with spatial variation in underlying edaphic and environmental conditions requiring high-resolution modeling. Second, increased spatial resolution enables improved attribution (Feng et al., 2022; Harris et al., 2016). Better locating of events on the land surface improves the ability to differentiate causes and consequences. Third, increased resolution is generally more relevant to local applications for policy and planning (Lamb et al., 2021). Land-use decisions and practices are often implemented at local scales because climate mitigation activities for terrestrial carbon relate directly to land ownership. Beyond the benefits of spatial resolution, linking process-based modeling with remote sensing has the added benefits of accuracy and inclusiveness. The remote sensing-based approach is likely more accurate based on increased use of direct observations of forest structure (Hurtt et al., 2019; Ma et al., 2021), and more inclusive because it

13652486, 2023, 12, Downloaded from https://onlinelibrary.wiley.com/doi/10.1111/gcb.16682 by Readcube (Labtiva Inc.), Wiley Online Library on [01/07/2024]. See the Terms and Conditions (https://onlinelibrary.wiley.com/terms-and-conditions) on Wiley Online Library for rules of use; OA articles are governed by the applicable Creative Commons License

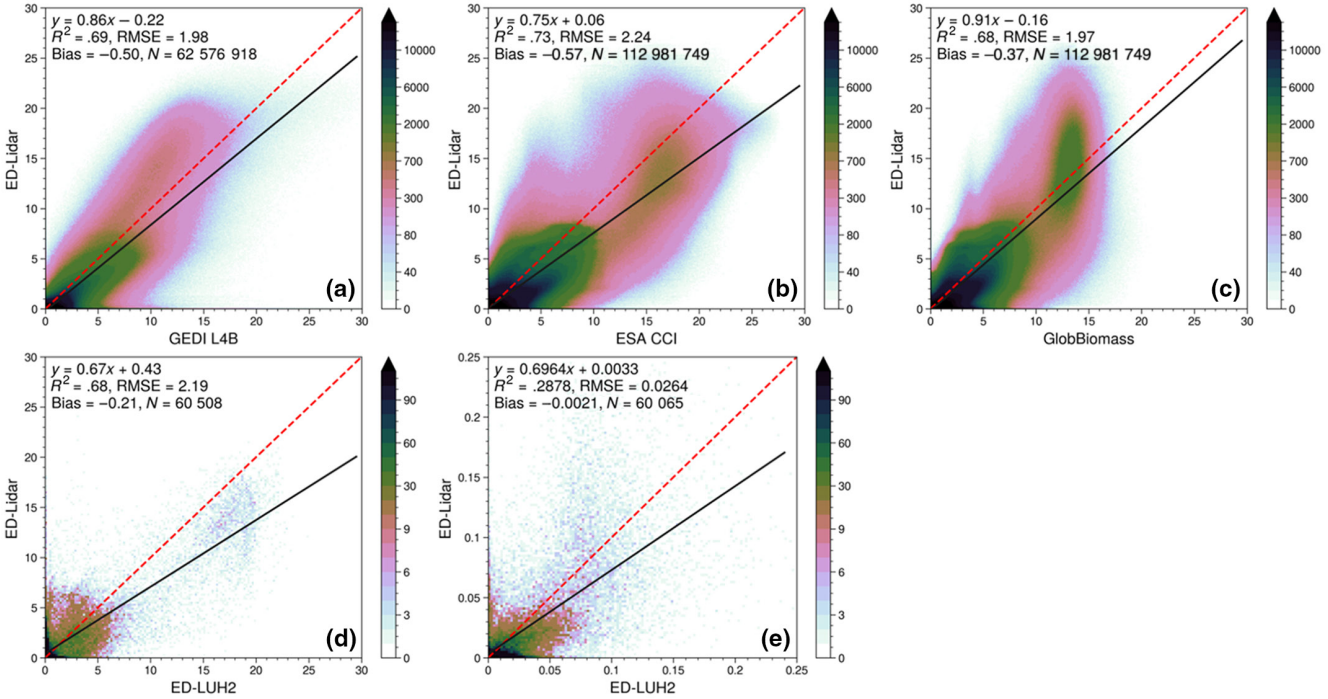

FIGURE 6 Comparison of carbon stocks and fluxes between ED-Lidar (GEDI and ICESat-2 combined) and those from GEDI L4B, ESA CCI, GlobBiomass, and ED-LUH2 at grid cell scale. (a–d) are comparisons of carbon stocks and (e) is comparison of carbon fluxes. Note that the comparison to GEDI L4B is limited to grid cells between 51°N and 51°S, and comparison to ED-LUH2 was at 0.5° scale. The other two comparisons were done at 0.01° over the globe.

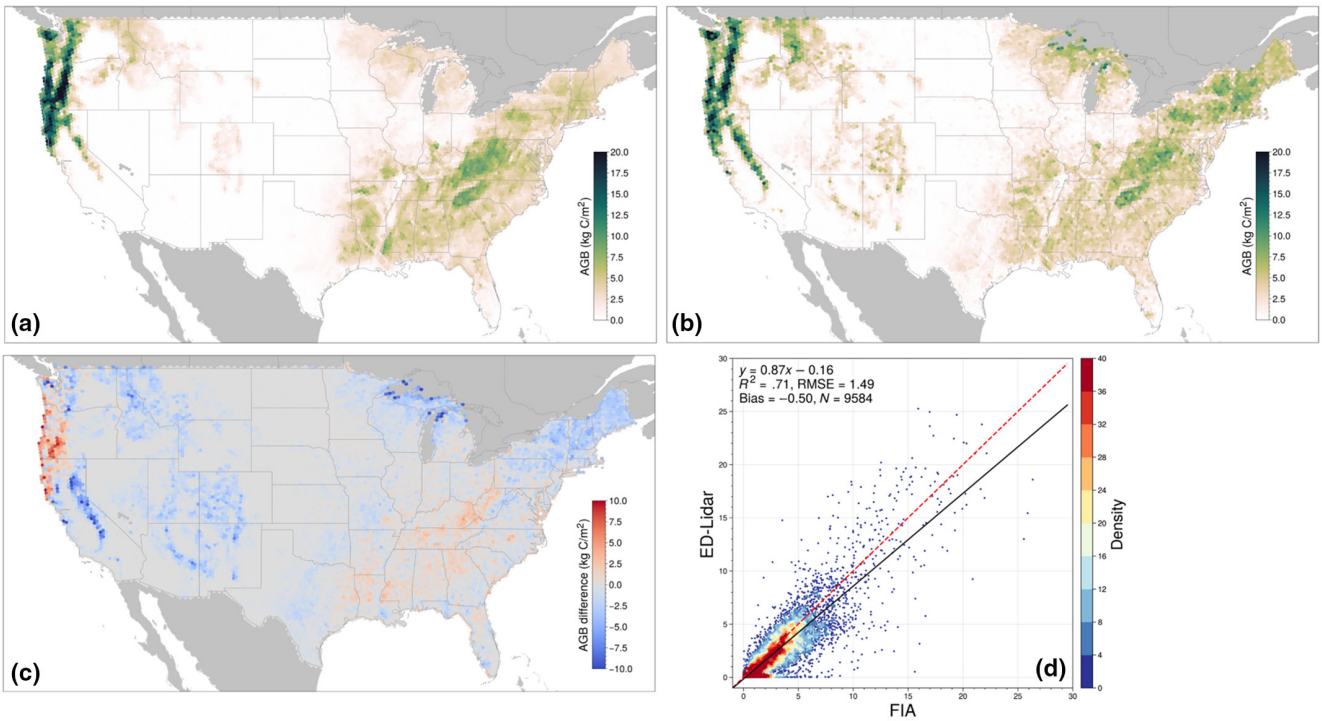

FIGURE 7 Comparison of hexagon average carbon stocks between estimates from ED-Lidar (GEDI and ICESat-2 combined) and the USFS FIA. (a) Hexagon-scale average from ED-Lidar; (b) hexagon-scale average from the USFS FIA; (c) difference map between (a) and (b); (d) scatter plot between (a) and (b).

13652486, 2023, 12, Downloaded from https://onlinelibrary.wiley.com/doi/10.1111/gcb.16682 by Readcube (Labtiva Inc.), Wiley Online Library on [01/07/2024]. See the Terms and Conditions (https://onlinelibrary.wiley.com/terms-and-conditions) on Wiley Online Library for rules of use; OA articles are governed by the applicable Creative Commons License

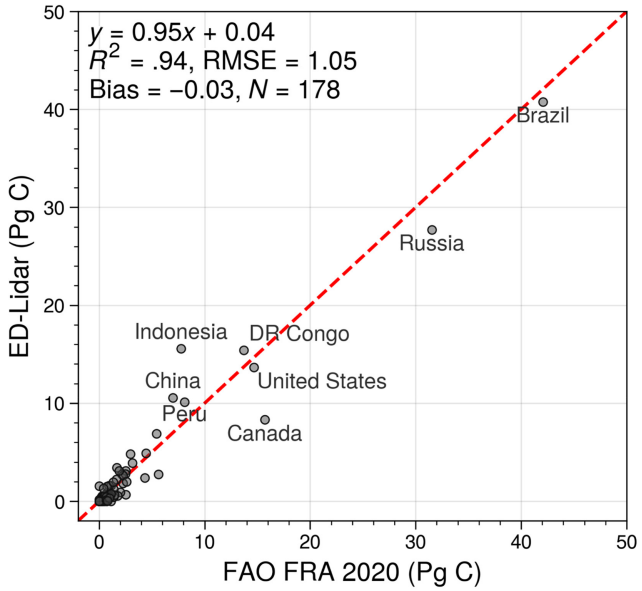

FIGURE 8 Comparison of estimates of total carbon stocks by country between estimates from ED-Lidar (GEDI and ICESat-2 combined) and FAO FRA 2020 reported values.

includes natural and anthropogenic effects (Frolking et al., 2009; Kent et al., 2015).

While the approach described here is based upon an unprecedented quantity of empirical forest structure observations in characterizing contemporary forest stocks and fluxes, several challenges remain with respect to input data and the modeling approach. On the input data side, this approach relies on high-quality data and broad spatial coverage. To maximize spatial coverage and sample density, lidar data used in this study came from two sources each providing sample coverage. This study compared model results using each lidar dataset alone and together. In general, using the two lidar sources together produced the best sample coverage and model results, but still resulted in areas of limited coverage and height differences (e.g., gridded average canopy height below 15 m and a seam line at ~latitude 51°N and 51°S because of the limit of GEDI coverage). However, uncertainties still exist when combining these datasets, and there remains a need for a harmonized canopy height dataset addressing related issues for global carbon modeling. In addition, it will be important to update global lidar data sets in the future to enable detailed model validation of height structured forest dynamics.

Despite uncertainties due to lidar input, we detected a powerful impact of vegetation structure data on constraining estimation of contemporary carbon stocks and fluxes. To illustrate this capability, potential carbon stocks and fluxes at early and late successional stages were estimated, representing the range from modeling processes without remote sensing observations being incorporated (Hurtt et al., 2004). Globally, results from this initialization produced estimates of contemporary carbon stocks and fluxes as 250.24 Pg C and 2.57 Pg C/year. ED-Lidar constrained carbon stocks to 32.21% of the maximum potential stocks, and carbon fluxes to 32.69% of maximum potential fluxes (Figure S8). Similar results were obtained from initialization using each lidar source alone (Tables 2 and 3). Note that the estimated carbon fluxes in this study were potential carbon fluxes, serving to isolate the impact of forest structure observations rather than to predict actual net fluxes, which in turn would depend on future transient meteorology and land-use activities.

This is the first study to produce consistent global estimates of forest aboveground carbon stocks and future potential net carbon fluxes at 0.01°, nearly 50 times finer than standard global carbon cycle modeling approaches at 0.5°. The approach, however, can be compared to other studies operating at this high spatial resolution that use empirically based methods, and to other ecosystem modeling studies using lidar. Several remote sensing/empirically based approaches have demonstrated the power of carbon mapping at high resolution (Baccini et al., 2012; Harris et al., 2021; Saatchi et al., 2011; Santoro, 2018; Wang et al., 2021; Xu et al., 2021). Many of these studies were based on the NASA Geoscience Laser Altimeter System (GLAS) which provided relatively sparse global lidar data sample coverage to the sources used here. Compared to these approaches, this study's approach adds process-based capabilities including the ability to project future fluxes as presented here. In comparison to other process-based models using lidar, important examples exist at regional scales. For example, studies using an ecosystem model called FORMIND have been completed using a different initialization approach (i.e., lidar waveform matching), for different spatial domain (i.e., tropical rainforests; Bauer et al., 2021; Knapp et al., 2018; Rödig et al., 2017, 2019).

Looking ahead, there are many areas for future research and advancement of terrestrial modeling using lidar. Next steps will leverage this work to develop forest carbon monitoring and modeling systems able to predict short-term carbon fluxes and project long-term carbon sequestration under alternative climate and land-use change scenarios. In the future, repeated global spaceborne lidar observations are needed to constrain such a system and will be necessary for ongoing calibration and assessment of model performance. The need for such future missions is articulated in the US Decadal Survey and there are several encouraging relevant missions in development (e.g., BIOMASS, NISAR; Board & National Research Council, 2007; NISAR, 2020; Quegan et al., 2019). In parallel, continued global mechanistic model development and refinement is needed to ensure maximum use of these data.

ACKNOWLEDGMENTS

This work was funded by NASA Carbon Monitoring System (NASA-CMS) project (80NSSC21K1059). RD, JA, LD, and SH received support from NASA Contract (#NNL15AA03C) for the development and execution of the GEDI mission. SH received support from GEDI ST grant (80HQTR21T0013). The authors are thankful to the Editor and Reviewers, whose comments helped us to improve the clarity of the article.

CONFLICT OF INTEREST STATEMENT

The authors have no conflict of interest to declare.

13652486, 2023, 12, Downloaded from https://onlinelibrary.wiley.com/doi/10.1111/gcb.16682 by Readcube (Labtiva Inc.), Wiley Online Library on [01/07/2024]. See the Terms and Conditions (https://onlinelibrary.wiley.com/terms-and-conditions) on Wiley Online Library for rules of use; OA articles are governed by the applicable Creative Commons License

DATA AVAILABILITY STATEMENT

The derived carbon estimates are available through https://doi.org/10.3334/ORNLDAAC/2180. The input drivers were from NASA GES DISC (https://disc.gsfc.nasa.gov/), NOAA CarbonTracker (https://gml.noaa.gov/ccgg/carbontracker/), and PANGAEA (https://doi.pangaea.de/10.1594/PANGAEA.870605). GEDI and ICESat-2 datasets were from NASA LPDAAC (https://lpdaac.usgs.gov/) and NASA ORNL DAAC (https://daac.ornl.gov/), and the CGLS dataset was from https://land.copernicus.eu/global/products/lc. Datasets used for the evaluation were from GlobBiomass (https://globbiomass.org/wp-content/uploads/GB_Maps/Globbiomass_global_dataset.html), the ESA CCI (https://climate.esa.int/en/projects/biomass/), the USGS FIA (https://zenodo.org/record/4294490#.ZAjKLezMLX1), the FAO FRA (https://www.fao.org/forest-resources-assessment/en/).

ORCID

Lei Ma https://orcid.org/0000-0002-3959-4155
Benjamin Poulter https://orcid.org/0000-0002-9493-8600
Quan Shen https://orcid.org/0000-0002-0654-0978

REFERENCES

Ahlström, A., Schurgers, G., Arneth, A., & Smith, B. (2012). Robustness and uncertainty in terrestrial ecosystem carbon response to CMIP5 climate change projections. *Environmental Research Letters*, *7*(4), 044008.

Anav, A., Friedlingstein, P., Kidston, M., Bopp, L., Ciais, P., Cox, P., Jones, C., Jung, M., Myneni, R., & Zhu, Z. (2013). Evaluating the land and ocean components of the global carbon cycle in the CMIP5 earth system models. *Journal of Climate*, *26*(18), 6801–6843.

Antonarakis, A. S., Saatchi, S. S., Chazdon, R. L., & Moorcroft, P. R. (2011). Using Lidar and Radar measurements to constrain predictions of forest ecosystem structure and function. *Ecological Applications*, *21*(4), 1120–1137.

Arima, E. Y., Walker, R. T., Perz, S., & Souza, C. (2016). Explaining the fragmentation in the Brazilian Amazonian forest. *Journal of Land Use Science*, *11*(3), 257–277. https://doi.org/10.1080/1747423X.2015.1027797

Baccini, A., Goetz, S., Walker, W., Laporte, N., Sun, M., Sulla-Menashe, D., Hackler, J., Beck, P., Dubayah, R., & Friedl, M. (2012). Estimated carbon dioxide emissions from tropical deforestation improved by carbon-density maps. *Nature Climate Change*, *2*(3), 182–185.

Bauer, L., Knapp, N., & Fischer, R. (2021). Mapping Amazon forest productivity by fusing GEDI Lidar waveforms with an individual-based forest model. *Remote Sensing*, *13*(22), Article 22. https://doi.org/10.3390/rs13224540

Board, S. S., & National Research Council. (2007). *Earth science and applications from space: National imperatives for the next decade and beyond*. National Academies Press.

Botkin, D. B., Janak, J. F., & Wallis, J. R. (1972). Some ecological consequences of a computer model of forest growth. *Journal of Ecology*, *60*(3), 849–872. https://doi.org/10.2307/2258570

Buchhorn, M., Smets, B., Bertels, L., Roo, B. D., Lesiv, M., Tsendbazar, N.-E., Herold, M., & Fritz, S. (2020). *Copernicus global land service: Land cover 100m: Collection 3: Epoch 2019: Globe* [data set]. Zenodo. https://doi.org/10.5281/zenodo.3939050

Chini, L., Hurtt, G., Sahajpal, R., Frolking, S., Klein Goldewijk, K., Sitch, S., Ganzenmüller, R., Ma, L., Ott, L., Pongratz, J., & Poulter, B. (2021). Land-use harmonization datasets for annual global carbon budgets. *Earth System Science Data*, *13*(8), 4175–4189. https://doi.org/10.5194/essd-13-4175-2021

Drake, J. B., Dubayah, R. O., Clark, D. B., Knox, R. G., Blair, J. B., Hofton, M. A., Chazdon, R. L., Weishampel, J. F., & Prince, S. (2002). Estimation of tropical forest structural characteristics using large-footprint lidar. *Remote Sensing of Environment*, *79*(2), 305–319. https://doi.org/10.1016/S0034-4257(01)00281-4

Dubayah, R., Blair, J. B., Goetz, S., Fatoyinbo, L., Hansen, M., Healey, S., Hofton, M., Hurtt, G., Kellner, J., & Luthcke, S. (2020). The global ecosystem dynamics investigation: High-resolution laser ranging of the Earth's forests and topography. *Science of Remote Sensing*, *1*, 100002.

Dubayah, R., Hofton, M., Blair, J., Armston, J., Tang, H., & Luthcke, S. (2021). GEDI L2A elevation and height metrics data global footprint level V002 [data set]. *NASA EOSDIS Land Processes DAAC*. https://doi.org/10.5067/GEDI/GEDI02_A.002

Dubayah, R. O., Armston, J., Healey, S. P., Yang, Z., Patterson, P. L., Saarela, S., Stahl, G., Duncanson, L., & Kellner, J. R. (2022). *Global ecosystem dynamics investigation (GEDI) GEDI L4B gridded aboveground biomass density, version 2* [GTiff]. https://doi.org/10.3334/ORNLDAAC/2017

Dubayah, R. O., & Drake, J. B. (2000). Lidar remote sensing for forestry. *Journal of Forestry*, *98*(6), 44–46. https://doi.org/10.1093/jof/98.6.44

Dubayah, R. O., Sheldon, S. L., Clark, D. B., Hofton, M. A., Blair, J. B., Hurtt, G. C., & Chazdon, R. L. (2010). Estimation of tropical forest height and biomass dynamics using lidar remote sensing at La Selva, Costa Rica. *Journal of Geophysical Research: Biogeosciences*, *115*(G2). https://doi.org/10.1029/2009JG000933

Eyring, V., Bony, S., Meehl, G. A., Senior, C. A., Stevens, B., Stouffer, R. J., & Taylor, K. E. (2016). Overview of the coupled model Intercomparison project phase 6 (CMIP6) experimental design and organization. *Geoscientific Model Development*, *9*(5), 1937–1958. https://doi.org/10.5194/gmd-9-1937-2016

FAO. (2020). *Global Forest Resources Assessment 2020: Main report*. FAO. https://doi.org/10.4060/ca9825en

Feng, Y., Zeng, Z., Searchinger, T. D., Ziegler, A. D., Wu, J., Wang, D., He, X., Elsen, P. R., Ciais, P., Xu, R., Guo, Z., Peng, L., Tao, Y., Spracklen, D. V., Holden, J., Liu, X., Zheng, Y., Xu, P., Chen, J., … Zheng, C. (2022). Doubling of annual forest carbon loss over the tropics during the early twenty-first century. *Nature Sustainability*, *5*(5), 444–451. https://doi.org/10.1038/s41893-022-00854-3

Fisher, R. A., Koven, C. D., Anderegg, W. R., Christoffersen, B. O., Dietze, M. C., Farrior, C. E., Holm, J. A., Hurtt, G. C., Knox, R. G., & Lawrence, P. J. (2018). Vegetation demographics in earth system models: A review of progress and priorities. *Global Change Biology*, *24*(1), 35–54.

Fisk, J., Hurtt, G., Chambers, J., Zeng, H., Dolan, K., & Negrón-Juárez, R. (2013). The impacts of tropical cyclones on the net carbon balance of eastern US forests (1851–2000). *Environmental Research Letters*, *8*(4), 045017.

Flanagan, S., Hurtt, G., Fisk, J., Sahajpal, R., Hansen, M., Dolan, K., Sullivan, J., & Zhao, M. (2016). Potential vegetation and carbon redistribution in northern North America from climate change. *Climate*, *4*(1), 2.

Friedlingstein, P., Jones, M. W., O'Sullivan, M., Andrew, R. M., Bakker, D. C. E., Hauck, J., Le Quéré, C., Peters, G. P., Peters, W., Pongratz, J., Sitch, S., Canadell, J. G., Ciais, P., Jackson, R. B., Alin, S. R., Anthoni, P., Bates, N. R., Becker, M., Bellouin, N., … Zeng, J. (2022). Global carbon budget 2021. *Earth System Science Data*, *14*(4), 1917–2005. https://doi.org/10.5194/essd-14-1917-2022

Frolking, S., Palace, M. W., Clark, D. B., Chambers, J. Q., Shugart, H. H., & Hurtt, G. C. (2009). Forest disturbance and recovery: A general review in the context of spaceborne remote sensing of impacts on aboveground biomass and canopy structure. *Journal of Geophysical Research: Biogeosciences*, *114*(G2). https://doi.org/10.1029/2008JG000911

13652486, 2023, 12, Downloaded from https://onlinelibrary.wiley.com/doi/10.1111/gcb.16682 by Readcube (Labtiva Inc.), Wiley Online Library on [01/07/2024]. See the Terms and Conditions (https://onlinelibrary.wiley.com/terms-and-conditions) on Wiley Online Library for rules of use; OA articles are governed by the applicable Creative Commons License

Gelaro, R., McCarty, W., Suárez, M. J., Todling, R., Molod, A., Takacs, L., Randles, C. A., Darmenov, A., Bosilovich, M. G., Reichle, R., Wargan, K., Coy, L., Cullather, R., Draper, C., Akella, S., Buchard, V., Conaty, A., da Silva, A. M., Gu, W., … Zhao, B. (2017). The modern-era retrospective analysis for research and applications, version 2 (MERRA-2). *Journal of Climate*, *30*(14), 5419–5454. https://doi.org/10.1175/JCLI-D-16-0758.1

Harris, N. L., Gibbs, D. A., Baccini, A., Birdsey, R. A., de Bruin, S., Farina, M., Fatoyinbo, L., Hansen, M. C., Herold, M., Houghton, R. A., Potapov, P. V., Suarez, D. R., Roman-Cuesta, R. M., Saatchi, S. S., Slay, C. M., Turubanova, S. A., & Tyukavina, A. (2021). Global maps of twenty-first century forest carbon fluxes. *Nature Climate Change*, *11*(3), 234–240. https://doi.org/10.1038/s41558-020-00976-6

Harris, N. L., Hagen, S. C., Saatchi, S. S., Pearson, T. R. H., Woodall, C. W., Domke, G. M., Braswell, B. H., Walters, B. F., Brown, S., Salas, W., Fore, A., & Yu, Y. (2016). Attribution of net carbon change by disturbance type across forest lands of the conterminous United States. *Carbon Balance and Management*, *11*(1), 24. https://doi.org/10.1186/s13021-016-0066-5

Houghton, R. A. (2003). Why are estimates of the terrestrial carbon balance so different? *Global Change Biology*, *9*(4), 500–509. https://doi.org/10.1046/j.1365-2486.2003.00620.x

Houghton, R. A. (2020). Terrestrial fluxes of carbon in GCP carbon budgets. *Global Change Biology*, *26*(5), 3006–3014. https://doi.org/10.1111/gcb.15050

Huang, W., Dolan, K., Swatantran, A., Johnson, K., Tang, H., O'Neil-Dunne, J., Dubayah, R., & Hurtt, G. (2019). High-resolution mapping of aboveground biomass for forest carbon monitoring system in the tri-state region of Maryland, Pennsylvania and Delaware, USA. *Environmental Research Letters*, *14*(9), 095002. https://doi.org/10.1088/1748-9326/ab2917

Hurtt, G., Chini, L., Sahajpal, R., Frolking, S., Bodirsky, B. L., Calvin, K., Doelman, J. C., Fisk, J., Fujimori, S., Klein Goldewijk, K., Hasegawa, T., Havlik, P., Heinimann, A., Humpenöder, F., Jungclaus, J., Kaplan, J. O., Kennedy, J., Krisztin, T., Lawrence, D., … Zhang, X. (2020). Harmonization of global land use change and management for the period 850–2100 (LUH2) for CMIP6. *Geoscientific Model Development*, *13*(11), 5425–5464. https://doi.org/10.5194/gmd-13-5425-2020

Hurtt, G., Chini, L. P., Frolking, S., Betts, R. A., Feddema, J., Fischer, G., Fisk, J. P., Hibbard, K., Houghton, R. A., & Janetos, A. (2011). Harmonization of land-use scenarios for the period 1500–2100: 600 years of global gridded annual land-use transitions, wood harvest, and resulting secondary lands. *Climatic Change*, *109*(1–2), 117–161.

Hurtt, G., Dubayah, R., Drake, J., Moorcroft, P. R., Pacala, S. W., Blair, J. B., & Fearon, M. G. (2004). Beyond potential vegetation: Combining Lidar data and a height-structured model for carbon studies. *Ecological Applications*, *14*(3), 873–883. https://doi.org/10.1890/02-5317

Hurtt, G., Fisk, J., Thomas, R., Dubayah, R., Moorcroft, P., & Shugart, H. (2010). Linking models and data on vegetation structure. *Journal of Geophysical Research: Biogeosciences*, *115*(G2). https://doi.org/10.1029/2009JG000937

Hurtt, G., Frolking, S., Fearon, M., Moore, B., Shevliakova, E., Malyshev, S., Pacala, S., & Houghton, R. (2006). The underpinnings of land-use history: Three centuries of global gridded land-use transitions, wood-harvest activity, and resulting secondary lands. *Global Change Biology*, *12*(7), 1208–1229.

Hurtt, G., Moorcroft, P., Pacala, S. W., & Levin, S. A. (1998). Terrestrial models and global change: Challenges for the future. *Global Change Biology*, *4*(5), 581–590.

Hurtt, G., Pacala, S. W., Moorcroft, P. R., Caspersen, J., Shevliakova, E., Houghton, R. A., & Moore, B. (2002). Projecting the future of the US carbon sink. *Proceedings of the National Academy of Sciences of the United States of America*, *99*(3), 1389–1394.

Hurtt, G., Thomas, R., Fisk, J., Dubayah, R., & Sheldon, S. (2016). The impact of fine-scale disturbances on the predictability of vegetation dynamics and carbon flux. *PLoS ONE*, *11*(4), e0152883.

Hurtt, G., Zhao, M., Sahajpal, R., Armstrong, A., Birdsey, R., Campbell, E., Dolan, K., Dubayah, R., Fisk, J., & Flanagan, S. (2019). Beyond MRV: High-resolution forest carbon modeling for climate mitigation planning over Maryland, USA. *Environmental Research Letters*, *14*(4), 045013.

Jacobson, A. R., Schuldt, K. N., Miller, J. B., Oda, T., Tans, P., Andrews, A., Mund, J., Ott, L., Collatz, G. J., Aalto, T., Afshar, S., Aikin, K., Aoki, S., Apadula, F., Baier, B., Bergamaschi, P., Beyersdorf, A., Biraud, S. C., Bollenbacher, A., … Zimnoch, M. (2020). Carbontracker CT2019B. https://doi.org/10.25925/20201008

Jones, C. D., Arora, V., Friedlingstein, P., Bopp, L., Brovkin, V., Dunne, J., Graven, H., Hoffman, F., Ilyina, T., John, J. G., Jung, M., Kawamiya, M., Koven, C., Pongratz, J., Raddatz, T., Randerson, J. T., & Zaehle, S. (2016). C4MIP—The coupled climate–carbon cycle model intercomparison project: Experimental protocol for CMIP6. *Geoscientific Model Development*, *9*(8), 2853–2880. https://doi.org/10.5194/gmd-9-2853-2016

Kent, R., Lindsell, J. A., Laurin, G. V., Valentini, R., & Coomes, D. A. (2015). Airborne LiDAR detects selectively logged tropical forest even in an advanced stage of recovery. *Remote Sensing*, *7*(7), 8348–8367. https://doi.org/10.3390/rs70708348

Knapp, N., Fischer, R., & Huth, A. (2018). Linking lidar and forest modeling to assess biomass estimation across scales and disturbance states. *Remote Sensing of Environment*, *205*, 199–209. https://doi.org/10.1016/j.rse.2017.11.018

Krause, A., Arneth, A., Anthoni, P., & Rammig, A. (2020). Legacy effects from historical environmental changes dominate future terrestrial carbon uptake. *Earth's Futures*, *8*(10), e2020EF001674. https://doi.org/10.1029/2020EF001674

Lamb, R. L., Hurtt, G. C., Boudreau, T. J., Campbell, E., Carlo, E. A. S., Chu, H.-H., de Mooy, J., Dubayah, R. O., Gonsalves, D., Guy, M., Hultman, N. E., Lehman, S., Leon, B., Lister, A. J., Lynch, C., Ma, L., Martin, C., Robbins, N., Rudee, A., … Tang, H. (2021). Context and future directions for integrating forest carbon into sub-national climate mitigation planning in the RGGI region of the U.S. *Environmental Research Letters*, *16*(6), 063001. https://doi.org/10.1088/1748-9326/abe6c2

Lawrence, D. M., Hurtt, G. C., Calvin, K. V., Jones, A. D., Jones, C. D., Lawrence, P. J., & Seneviratne, S. I. (2016). The land use model Intercomparison project (LUMIP) contribution to CMIP6: Rationale and experimental design. *Geoscientific Model Development*, *9*(9), 2973–2998.

Liu, J., Coomes, D. A., Gibson, L., Hu, G., Liu, J., Luo, Y., Wu, C., & Yu, M. (2019). Forest fragmentation in China and its effect on biodiversity. *Biological Reviews*, *94*(5), 1636–1657. https://doi.org/10.1111/brv.12519

Liu, S., Bond-Lamberty, B., Hicke, J. A., Vargas, R., Zhao, S., Chen, J., Edburg, S. L., Hu, Y., Liu, J., McGuire, A. D., Xiao, J., Keane, R., Yuan, W., Tang, J., Luo, Y., Potter, C., & Oeding, J. (2011). Simulating the impacts of disturbances on forest carbon cycling in North America: Processes, data, models, and challenges. *Journal of Geophysical Research: Biogeosciences*, *116*(G4). https://doi.org/10.1029/2010JG001585

Longo, M., Knox, R. G., Medvigy, D. M., Levine, N. M., Dietze, M. C., Kim, Y., Swann, A. L. S., Zhang, K., Rollinson, C. R., Bras, R. L., Wofsy, S. C., & Moorcroft, P. R. (2019). The biophysics, ecology, and biogeochemistry of functionally diverse, vertically and horizontally heterogeneous ecosystems: The ecosystem demography model, version 2.2—Part 1: Model description. *Geoscientific Model Development*, *12*(10), 4309–4346. https://doi.org/10.5194/gmd-12-4309-2019

Los, S. O., Rosette, J. A. B., Kljun, N., North, P. R. J., Chasmer, L., Suárez, J. C., Hopkinson, C., Hill, R. A., van Gorsel, E., Mahoney, C., & Berni, J. A. J. (2012). Vegetation height and cover fraction between 60°S and 60°N from ICESat GLAS data. *Geoscientific Model Development*, *5*(2), 413–432. https://doi.org/10.5194/gmd-5-413-2012

Ma, L., Hurtt, G., Ott, L., Sahajpal, R., Fisk, J., Lamb, R., Tang, H., Flanagan, S., Chini, L., Chatterjee, A., & Sullivan, J. (2022). Global evaluation of the ecosystem

13652486, 2023, 12, Downloaded from https://onlinelibrary.wiley.com/doi/10.1111/gcb.16682 by Readcube (Labtiva Inc.), Wiley Online Library on [01/07/2024]. See the Terms and Conditions (https://onlinelibrary.wiley.com/terms-and-conditions) on Wiley Online Library for rules of use; OA articles are governed by the applicable Creative Commons License

demography model (ED v3.0). *Geoscientific Model Development*, *15*(5), 1971–1994. https://doi.org/10.5194/gmd-15-1971-2022

Ma, L., Hurtt, G., Tang, H., Lamb, R., Campbell, E., Dubayah, R., Guy, M., Huang, W., Lister, A., Lu, J., O'Neil-Dunne, J., Rudee, A., Shen, Q., & Silva, C. (2021). High-resolution forest carbon modelling for climate mitigation planning over the RGGI region, USA. *Environmental Research Letters*, *16*(4), 045014. https://doi.org/10.1088/1748-9326/abe4f4

Ma, L., Hurtt, G. C., Chini, L. P., Sahajpal, R., Pongratz, J., Frolking, S., Stehfest, E., Klein Goldewijk, K., O'Leary, D., & Doelman, J. C. (2020). Global rules for translating land-use change (LUH2) to land-cover change for CMIP6 using GLM2. *Geoscientific Model Development*, *13*(7), 3203–3220. https://doi.org/10.5194/gmd-13-3203-2020

Markus, T., Neumann, T., Martino, A., Abdalati, W., Brunt, K., Csatho, B., Farrell, S., Fricker, H., Gardner, A., Harding, D., Jasinski, M., Kwok, R., Magruder, L., Lubin, D., Luthcke, S., Morison, J., Nelson, R., Neuenschwander, A., Palm, S., … Zwally, J. (2017). The ice, cloud, and land elevation Satellite-2 (ICESat-2): Science requirements, concept, and implementation. *Remote Sensing of Environment*, *190*, 260–273. https://doi.org/10.1016/j.rse.2016.12.029

McGuire, A. D., Sitch, S., Clein, J. S., Dargaville, R., Esser, G., Foley, J., Heimann, M., Joos, F., Kaplan, J., Kicklighter, D. W., Meier, R. A., Melillo, J. M., Moore, B., III, Prentice, I. C., Ramankutty, N., Reichenau, T., Schloss, A., Tian, H., Williams, L. J., & Wittenberg, U. (2001). Carbon balance of the terrestrial biosphere in the twentieth century: Analyses of CO_2, climate and land use effects with four process-based ecosystem models. *Global Biogeochemical Cycles*, *15*(1), 183–206. https://doi.org/10.1029/2000GB001298

MDE. (2021). *The greenhouse gas emissions reduction act*. The Maryland Department of the Environment. https://mde.maryland.gov/programs/air/ClimateChange/Documents/2030%20GGRA%20Plan/THE%202030%20GGRA%20PLAN.pdf

MDE. (2022). *Reducing greenhouse gas emissions in Maryland: A progress report*. The Maryland Department of the Environment. https://mde.maryland.gov/programs/air/ClimateChange/Documents/GGRA%20PROGRESSS%20REPORT%202022.pdf

Medvigy, D., Wofsy, S. C., Munger, J. W., Hollinger, D. Y., & Moorcroft, P. R. (2009). Mechanistic scaling of ecosystem function and dynamics in space and time: Ecosystem demography model version 2. *Journal of Geophysical Research: Biogeosciences*, *114*(G1). https://doi.org/10.1029/2008JG000812

Menlove, J., & Healey, S. P. (2020). A comprehensive forest biomass dataset for the USA allows customized validation of remotely sensed biomass estimates. *Remote Sensing*, *12*(24), 4141. https://doi.org/10.3390/rs12244141

Montzka, C., Herbst, M., Weihermüller, L., Verhoef, A., & Vereecken, H. (2017). A global data set of soil hydraulic properties and sub-grid variability of soil water retention and hydraulic conductivity curves. *Earth System Science Data*, *9*(2), 529–543. https://doi.org/10.5194/essd-9-529-2017

Moorcroft, P. R., Hurtt, G. C., & Pacala, S. W. (2001). A method for scaling vegetation dynamics: The ecosystem demography model (ED). *Ecological Monographs*, *71*(4), 557–586.

Neuenschwander, A., & Pitts, K. (2019). The ATL08 land and vegetation product for the ICESat-2 Mission. *Remote Sensing of Environment*, *221*, 247–259.

Neuenschwander, A. L., Pitts, K. L., Jelley, B. P., Robbins, J., Klotz, B., Popescu, S. C., Nelson, R. F., Harding, D., Pederson, D., & Sheridan, R. (2021). *ATLAS/ICESat-2 L3A land and vegetation height, version 5* [Indicate subset used]. NASA National Snow and Ice Data Center Distributed Active Archive Center. https://doi.org/10.5067/ATLAS/ATL08.005

NISAR. (2020). *NISAR*. NASA-ISRO SAR Mission (NISAR). https://nisar.jpl.nasa.gov/

Oliveras, I., & Malhi, Y. (2016). Many shades of green: The dynamic tropical forest–Savannah transition zones. *Philosophical Transactions of the Royal Society B: Biological Sciences*, *371*(1703), 20150308. https://doi.org/10.1098/rstb.2015.0308

Prentice, I. C., Bondeau, A., Cramer, W., Harrison, S. P., Hickler, T., Lucht, W., Sitch, S., Smith, B., & Sykes, M. T. (2007). Dynamic global vegetation modeling: Quantifying terrestrial ecosystem responses to large-scale environmental change. In J. G. Canadell, D. E. Pataki, & L. F. Pitelka (Eds.), *Terrestrial ecosystems in a changing world* (pp. 175–192). Springer. https://doi.org/10.1007/978-3-540-32730-1_15

Quegan, S., Le Toan, T., Chave, J., Dall, J., Exbrayat, J.-F., Minh, D. H. T., Lomas, M., D'Alessandro, M. M., Paillou, P., Papathanassiou, K., Rocca, F., Saatchi, S., Scipal, K., Shugart, H., Smallman, T. L., Soja, M. J., Tebaldini, S., Ulander, L., Villard, L., & Williams, M. (2019). The European Space Agency BIOMASS mission: Measuring forest above-ground biomass from space. *Remote Sensing of Environment*, *227*, 44–60. https://doi.org/10.1016/j.rse.2019.03.032

Quesada, B., Arneth, A., Robertson, E., & de Noblet-Ducoudré, N. (2018). Potential strong contribution of future anthropogenic land-use and land-cover change to the terrestrial carbon cycle. *Environmental Research Letters*, *13*(6), 064023. https://doi.org/10.1088/1748-9326/aac4c3

Riitters, K. H., Wickham, J. D., O'Neill, R. V., Jones, K. B., Smith, E. R., Coulston, J. W., Wade, T. G., & Smith, J. H. (2002). Fragmentation of continental United States forests. *Ecosystems*, *5*(8), 815–822. https://doi.org/10.1007/s10021-002-0209-2

Rödig, E., Cuntz, M., Heinke, J., Rammig, A., & Huth, A. (2017). Spatial heterogeneity of biomass and forest structure of the Amazon rain forest: Linking remote sensing, forest modelling and field inventory. *Global Ecology and Biogeography*, *26*(11), 1292–1302. https://doi.org/10.1111/geb.12639

Rödig, E., Knapp, N., Fischer, R., Bohn, F. J., Dubayah, R., Tang, H., & Huth, A. (2019). From small-scale forest structure to Amazon-wide carbon estimates. *Nature Communications*, *10*(1), 5088. https://doi.org/10.1038/s41467-019-13063-y

Saatchi, S. S., Harris, N. L., Brown, S., Lefsky, M., Mitchard, E. T., Salas, W., Zutta, B. R., Buermann, W., Lewis, S. L., & Hagen, S. (2011). Benchmark map of forest carbon stocks in tropical regions across three continents. *Proceedings of the National Academy of Sciences of the United States of America*, *108*(24), 9899–9904.

Saldarriaga, J. G., West, D. C., Tharp, M. L., & Uhl, C. (1988). Long-term Chronosequence of Forest succession in the upper Rio Negro of Colombia and Venezuela. *Journal of Ecology*, *76*(4), 938–958. https://doi.org/10.2307/2260625

Santoro, M. (2018). *GlobBiomass—Global datasets of forest biomass* [data set]. Pangaea. https://doi.org/10.1594/PANGAEA.894711

Santoro, M., & Cartus, O. (2021). *ESA biomass climate change initiative (biomass_cci): Global datasets of forest above-ground biomass for the years 2010, 2017 and 2018, v3 [Application/xml]*. NERC EDS Centre for Environmental Data Analysis. https://doi.org/10.5285/5F331C418E9F4935B8EB1B836F8A91B8

Scheiter, S., Langan, L., & Higgins, S. I. (2013). Next-generation dynamic global vegetation models: Learning from community ecology. *New Phytologist*, *198*(3), 957–969.

Shugart, H. (1984). *A theory of forest dynamics. The ecological implications of forest succession models*. Springer-Verlag. https://www.cabdirect.org/cabdirect/abstract/19850602322

Shugart, H., & West, D. C. (1977). Development of an Appalachian deciduous forest succession model and its application to assessment of the impact of the chestnut blight. *Journal of Environmental Management*, *5*(2), 161–179.

Sitch, S., Friedlingstein, P., Gruber, N., Jones, S. D., Murray-Tortarolo, G., Ahlström, A., Doney, S. C., Graven, H., Heinze, C., Huntingford, C., Levis, S., Levy, P. E., Lomas, M., Poulter, B., Viovy, N., Zaehle, S., Zeng, N., Arneth, A., Bonan, G., … Myneni, R. (2015). Recent trends and drivers of regional sources and sinks of carbon dioxide. *Biogeosciences*, *12*(3), 653–679. https://doi.org/10.5194/bg-12-653-2015

Sitch, S., Huntingford, C., Gedney, N., Levy, P. E., Lomas, M., Piao, S. L., Betts, R., Ciais, P., Cox, P., Friedlingstein, P., Jones, C. D.,

13652486, 2023, 12, Downloaded from https://onlinelibrary.wiley.com/doi/10.1111/gcb.16682 by Readcube (Labtiva Inc.), Wiley Online Library on [01/07/2024]. See the Terms and Conditions (https://onlinelibrary.wiley.com/terms-and-conditions) on Wiley Online Library for rules of use; OA articles are governed by the applicable Creative Commons License

Prentice, I. C., & Woodward, F. I. (2008). Evaluation of the terrestrial carbon cycle, future plant geography and climate-carbon cycle feedbacks using five dynamic global vegetation models (DGVMs). *Global Change Biology*, *14*(9), 2015–2039. https://doi.org/10.1111/j.1365-2486.2008.01626.x

Tang, H., Dubayah, R., Swatantran, A., Hofton, M., Sheldon, S., Clark, D. B., & Blair, B. (2012). Retrieval of vertical LAI profiles over tropical rain forests using waveform lidar at La Selva, Costa Rica. *Remote Sensing of Environment*, *124*, 242–250.

Tang, H., Ma, L., Lister, A., O'Neill-Dunne, J., Lu, J., Lamb, R. L., Dubayah, R., & Hurtt, G. (2021). High-resolution forest carbon mapping for climate mitigation baselines over the RGGI region, USA. *Environmental Research Letters*, *16*(3), 035011. https://doi.org/10.1088/1748-9326/abd2ef

Taylor, K. E., Stouffer, R. J., & Meehl, G. A. (2012). An overview of CMIP5 and the experiment design. *Bulletin of the American Meteorological Society*, *93*(4), 485–498. https://doi.org/10.1175/BAMS-D-11-00094.1

Thom, D., Rammer, W., Garstenauer, R., & Seidl, R. (2018). Legacies of past land use have a stronger effect on forest carbon exchange than future climate change in a temperate forest landscape. *Biogeosciences*, *15*(18), 5699–5713. https://doi.org/10.5194/bg-15-5699-2018

Thomas, R. Q., Hurtt, G. C., Dubayah, R., & Schilz, M. H. (2008). Using lidar data and a height-structured ecosystem model to estimate forest carbon stocks and fluxes over mountainous terrain. *Canadian Journal of Remote Sensing*, *34*(Supp. 2), S351–S363.

Wang, J. A., Baccini, A., Farina, M., Randerson, J. T., & Friedl, M. A. (2021). Disturbance suppresses the aboveground carbon sink in North American boreal forests. *Nature Climate Change*, *11*(5), 435–441. https://doi.org/10.1038/s41558-021-01027-4

Xu, L., Saatchi, S. S., Yang, Y., Yu, Y., Pongratz, J., Bloom, A. A., Bowman, K., Worden, J., Liu, J., Yin, Y., Domke, G., McRoberts, R. E., Woodall, C., Nabuurs, G.-J., de-Miguel, S., Keller, M., Harris, N., Maxwell, S., & Schimel, D. (2021). Changes in global terrestrial live biomass over the 21st century. *Science Advances*, *7*(27), eabe9829. https://doi.org/10.1126/sciadv.abe9829

Yang, H., Ciais, P., Santoro, M., Huang, Y., Li, W., Wang, Y., Bastos, A., Goll, D., Arneth, A., Anthoni, P., Arora, V. K., Friedlingstein, P., Harverd, V., Joetzjer, E., Kautz, M., Lienert, S., Nabel, J. E. M. S., O'Sullivan, M., Sitch, S., … Zhu, D. (2020). Comparison of forest above-ground biomass from dynamic global vegetation models with spatially explicit remotely sensed observation-based estimates. *Global Change Biology*, *26*(7), 3997–4012. https://doi.org/10.1111/gcb.15117

SUPPORTING INFORMATION

Additional supporting information can be found online in the Supporting Information section at the end of this article.

How to cite this article: Ma, L., Hurtt, G., Tang, H., Lamb, R., Lister, A., Chini, L., Dubayah, R., Armston, J., Campbell, E., Duncanson, L., Healey, S., O'Neil-Dunne, J., Ott, L., Poulter, B., & Shen, Q. (2023). Spatial heterogeneity of global forest aboveground carbon stocks and fluxes constrained by spaceborne lidar data and mechanistic modeling. *Global Change Biology*, *29*, 3378–3394. https://doi.org/10.1111/gcb.16682

13652486, 2023, 12, Downloaded from https://onlinelibrary.wiley.com/doi/10.1111/gcb.16682 by Readcube (Labtiva Inc.), Wiley Online Library on [01/07/2024]. See the Terms and Conditions (https://onlinelibrary.wiley.com/terms-and-conditions) on Wiley Online Library for rules of use; OA articles are governed by the applicable Creative Commons License